creative commons
COMMONS DEED

저작자표시-비영리-변경금지 2.0 대한민국

이용자는 아래의 조건을 따르는 경우에 한하여 자유롭게

- 이 저작물을 복제, 배포, 전송, 전시, 공연 및 방송할 수 있습니다.

다음과 같은 조건을 따라야 합니다:

저작자표시. 귀하는 원저작자를 표시하여야 합니다.

비영리. 귀하는 이 저작물을 영리 목적으로 이용할 수 없습니다.

변경금지. 귀하는 이 저작물을 개작, 변형 또는 가공할 수 없습니다.

- 귀하는, 이 저작물의 재이용이나 배포의 경우, 이 저작물에 적용된 이용허락조건을 명확하게 나타내어야 합니다.
- 저작권자로부터 별도의 허가를 받으면 이러한 조건들은 적용되지 않습니다.

저작권법에 따른 이용자의 권리는 위의 내용에 의하여 영향을 받지 않습니다.

이것은 이용허락규약(Legal Code)을 이해하기 쉽게 요약한 것입니다.

Disclaimer

dCollection

ULSAN NATIONAL INSTITUTE OF
SCIENCE AND TECHNOLOGY

Development of Small Molecules as Chemical Probes for Understanding the Pathology of Alzheimer's Disease

Misun Lee

Department of Chemistry

Graduate School of UNIST

ULSAN NATIONAL INSTITUTE OF
SCIENCE AND TECHNOLOGY

Development of Small Molecules as Chemical Probes for Understanding the Pathology of Alzheimer's Disease

A thesis submitted to the Graduate School of UNIST
in partial fulfillment of the requirements
for the degree of Master of Science

Misun Lee

12. 03. 2018
Approved by

Advisor
Associate Professor Oh-Hoon Kwon

ULSAN NATIONAL INSTITUTE OF SCIENCE AND TECHNOLOGY

Development of Small Molecules as Chemical Probes for Understanding the Pathology of Alzheimer's Disease

Misun Lee

This certifies that the thesis of Misun Lee is approved.

12. 03. 2018

Signature

Advisor: Associate Professor Oh-Hoon Kwon

Signature

Associate Professor: Mi Hee Lim

Signature

Assistant Professor: Jung-Min Kee

ULSAN NATIONAL INSTITUTE OF SCIENCE AND TECHNOLOGY

Abstract

Alzheimer's Disease (AD), responsible for most dementia cases, is one of the prevalent neurodegenerative diseases. Multiple features (*e.g.*, neuroinflammation, accumulation of amyloid aggregates, dyshomeostasis of metal ions) have been implicated in the pathogenesis of AD, and such multifactorial nature impedes the investigation of the effective treatment of the disease. To elucidate the unrevealed biological actions linked with the pathogenesis and identify the remedy for the disease, many studies have been focused on devising and utilizing small molecules as chemical probes or potential therapeutics. In Chapter 1, we describe the development of a small molecule, **1**, as a chemical agent for understanding the interconnection between neuroinflammation and amyloid-β (Aβ) peptides as well as a potential drug candidate against AD. By intervening in the inflammatory process of microglia, **1** could promote the microglial phagocytosis of Aβ and subsequently ameliorates cognitive defects *in vivo*. These results could provide an advanced insight to future discovery of effective anti-neuroinflammatory drugs against neurodegeneration. In Chapter 2, a turn-on near-infrared (near-IR) fluorescent probe, **2**, for imaging Aβ aggregates is introduced. The ability of **2** was evaluated to alter fluorescent response depending on the degree of Aβ aggregation, at the near-IR region, and its suitability for imaging Aβ aggregates under cellular environments. This work allows us to attain new perceptions to devise improved fluorescent probes with better specificity and bioapplicability, *via* further structural modifications. In Chapter 3, the design of small molecules capable of detecting metal ions in living cells is described. These studies present the capability of our molecules to monitor metal ions in living cells. Overall, our studies illustrate the utilization of small molecules to gain a better understanding of the pathogenic factors of interest, which will contribute to invention of chemical agents used for elucidating the pathology of AD.

ULSAN NATIONAL INSTITUTE OF SCIENCE AND TECHNOLOGY

Table of Contents

ULSAN NATIONAL INSTITUTE OF SCIENCE AND TECHNOLOGY

ULSAN NATIONAL INSTITUTE OF SCIENCE AND TECHNOLOGY

ULSAN NATIONAL INSTITUTE OF
SCIENCE AND TECHNOLOGY

List of Tables

ULSAN NATIONAL INSTITUTE OF SCIENCE AND TECHNOLOGY

List of Figures

ULSAN NATIONAL INSTITUTE OF SCIENCE AND TECHNOLOGY

mice. *P < 0.05; **P < 0.01 by One-way analysis of variance, Tukey's post hoc test. All error bars indicate s.e.m.

Figure 1.6. Identification of the responsible cells upon incubation of $A\beta_{42}$ with and without **1**. (a) Analysis of mRNA levels of inflammatory cytokines in microglia by treatment of $A\beta_{42}$ species with and without **1** or in astrocytes [grown by transferring the conditioned media (CM) harvested from the microglia] (n = 3 independent experiments). (b) Measurement of mRNA levels of inflammatory cytokines in astrocytes upon addition of $A\beta_{42}$ species with and without **1** or in microglia (grown by transferring the CM harvested from the astrocytes) (n = 3 independent experiments). (**c**) Determination of mRNA levels of off/on signals in neurons with incubation of $A\beta_{42}$ species with and without **1** or inflammatory cytokines in microglia (grown by transferring the CM harvested from the neurons) (n = 3 independent experiments). Conditions: [$A\beta_{42}$] = 10 μM; [**1**] = 10 μM; pro-inflammatory marker: TNF-α, IL-1β, IL-6, and iNOS; immunoregulatory cytokine: IL-10; anti-inflammatory marker: IL-4, TGF-β, and Arg1; off signals*:* BDNF, CD4, and CD200; on signals: CXCL10, CCL21, and MMP3. *P < 0.05; **P < 0.01 by One-way analysis of variance, Tukey's post hoc test. All error bars indicate s.e.m.

Figure 1.7. Analysis of the microglial phagocytosis of Aβ and the activity of NLRP3 inflammasome-related proteins in **1**-treated APP/PS1 mice. (a) Colocalization of the microglia (Iba1, red) with Aβ aggregates (ThS, green) and quantification. Scale bars = 10 μm. 3D reconstruction from confocal image stacks. Scale bars = 10 μm. (b) Immunofluorescence images of Aβ aggregates (ThS, green) encapsulated within phagolysosome (Lamp1, blue) in microglia (Iba1, red) in the brains of vehicle- or **1**-treated APP/PS1 mice. Quantification of the microglial volume occupied by Lamp1(+) phagolysosomes, percent of the microglia containing Aβ-loaded phagolysosome, and Aβ encapsulated in phagolysosomes. Low magnification scale bars = 40 μm; high magnification scale bars = 10 μm. 3D reconstruction from confocal image stacks. Scale bars = 10 μm. (c) Morphology of microglia (Iba1, red) surrounding Aβ (ThS, green) in the cortex of vehicle- or **1**-treated APP/PS1 mice. Scale bars = 10 μm. 3D reconstruction from confocal image stacks. (d) Morphometric analysis of Aβ plaques in vehicle- or **1**-treated APP/PS1 mice. (e) Effects of **1** on the activity of NLRP3 inflammasome-related proteins. Wild-type mice (WT), vehicle-treated APP/PS1 mice (vehicle), and **1**-treated APP/PS1 mice (**1**). All data analysis was done at 9.5 months of age. Animal number: (a-d) n = 3 for vehicle- or **1**-treated APP/PS1 mice; (e) n = 4 for WT mice and n = 4 for vehicle-treated or **1**-treated APP/PS1 mice. *P < 0.05; **P < 0.01 by Student's t test or One-way analysis of variance, Tukey's post hoc test. All error bars indicate s.e.m.

Figure 1.8. Effects of **1** on the aggregation of Aβ and the expression of Aβ-degrading enzymes. (a) Scheme of the (i) inhibition and (ii) disaggregation experiments. (b) Visualization of the size distribution of the resultant $A\beta_{40}$ and $A\beta_{42}$ species from (i) and (ii) by gel/Western blot using an anti-Aβ antibody (6E10). Lanes: (C) $A\beta_{40}$ or $A\beta_{42}$; (**1**) $A\beta_{40}$ or $A\beta_{42}$ + **1**. (c) TEM images of the samples obtained from (b, i). Scale bars = 200 nm. Conditions: [$A\beta_{40}$ or $A\beta_{42}$] = 25 μM; [**1**] = 50 μM; 20 mM HEPES, pH 7.4, 150 mM NaCl; 24 h; 37 °C; constant agitation. (d) Analysis of the levels of the enzymes (*i.e.*, NEP, MMP9, and IDE) involved in Aβ degradation in wild-type mice (WT) and vehicle- or **1**-administrated APP/PS1 mice (vehicle or **1**). All data analysis was done at 9.5 months of age. Animal number: (d) n = 4 for WT mice and n = 4 for vehicle- or **1**-treated APP/PS1 mice. *P < 0.05 by One-way analysis of variance, Tukey's post hoc test. All error bars indicate s.e.m.

ULSAN NATIONAL INSTITUTE OF SCIENCE AND TECHNOLOGY

ULSAN NATIONAL INSTITUTE OF SCIENCE AND TECHNOLOGY

Figure 3.1. Fluorescence imaging of HeLa cells incubated with **3** and Al^{3+}. Cells were pre-incubated with Al^{3+} for 20 min prior to addition of **3**. Conditions: [**3**] = 25 μM, [Al^{3+}] = 500 μM, 37 °C, 5% CO_2. Scale bars = 50 μm.

Figure 3.2. Fluorescence imaging of HeLa cells incubated with **4** and Zn^{2+}. Cells were incubated with **4** and Zn^{2+} for 5 min. Conditions: [**4**] = 10 μM; [Zn^{2+}] = 1 mM; 37 °C; 5% CO_2. Scale bars = 50 μm.

Figure 3.3. Toxicity of **4** incubated in HeLa cells for (a) 5 min and (b) 24 h. **4** was treated to HeLa cells at various concentration (5, 10, 20, and 50 μM; 1% v/v DMSO). Cell viability (%) was determined by the MTT assay [MTT = 3-(4,5-dimethylthiazol-2-yl)-2,5-diphenyltetrazolium bromide] in comparison to that of cells treated with DMSO only (1% v/v). Error bars represent the standard error from three independent experiments.

Figure 3.4. Fluorescence images of HeLa cells incubated with **5** followed by the addition of Zn^{2+}. Cells were treated with **5** for 90 min prior to the introduction of Zn^{2+}. Conditions: [**5**] = 25 μM; [Zn^{2+}] = 0.5 or 1 mM; 37 °C; 5% CO_2. Scale bars = 50 μm.

ULSAN NATIONAL INSTITUTE OF SCIENCE AND TECHNOLOGY

List of Schemes

ULSAN NATIONAL INSTITUTE OF SCIENCE AND TECHNOLOGY

List of Abbreviations

AD	Alzheimer's disease
Aβ	Amyloid-β
Near-IR	Near-infrared
CNS	Central nervous system
NLRP3	NACHT, LRR, and PYD domains-containing protein 3
MTT	3-(4,5-Dimethylthiazol-2-yl)-2,5-diphenyltetrazolium bromide
BBB	Blood-brain barrier
DMSO	Dimethyl sulfoxide
NMR	Nuclear magnetic resonance
WT	Wild-type
MWM	Morris water maze
ThS	Thioflavin-S
s.e.m.	Standard errors of mean
APP	Amyloid precursor protein
PS1	Presenilin-1
i.p.	Intraperitoneal
Iba1	Ionized calcium-binding adapter molecule 1
GFAP	Glial fibrillary acidic protein
Lamp1	Lysosomal-associated membrane protein 1
CM	Conditioned media
TNF-α	Tumor necrosis factor-alpha
IL-1β	Interleukin-1β
IL-6	Interleukin-6
iNOS	Inducible nitric oxide synthase;
IL-10	Interleukin-10
IL-4	Interleukin-4
TGF-β	Transforming growth factor-β
Arg1	Arginase 1
CXCL10	Chemokine (C-X-C Motif) ligand 10
CCL21	Chemokine (C-C Motif) ligand 21
MMP3	Matrix metallopeptidase 3
CD47	Cluster of differentiation 47
BDNF	Brain-derived neurotrophic factor
CD200	Cluster of differentiation 200

ULSAN NATIONAL INSTITUTE OF SCIENCE AND TECHNOLOGY

NEP	Neprilysin
MMP9	Matrix metallopeptidase 9
IDE	Insulin degrading enzyme
GAPDH	Glyceraldehyde 3-phosphate dehydrogenase
ASC	Apoptosis-associated speck-like protein containing CARD
Gel/Western blot	Gel electrophoresis and Western blot
TEM	Transmission electron microscopy
UV−Vis	Ultraviolet–visible spectroscopy
DMF	Dimethylformamide
NADPH	Dihydronicotinamide adenine dinucleotide phosphate
CSF	Cerebrospinal fluid
PCR	Polymerase chain reaction
ELISA	Enzyme-linked immunosorbent assay
ThT	Thioflavin-T
GFP	Green fluorescent protein
DAPI	4′,6-Diamidino-2-phenylindole
ESI-MS	Electrospray ionization-mass spectrometry

ULSAN NATIONAL INSTITUTE OF SCIENCE AND TECHNOLOGY

Chapter 1.

A Small Synthetic Molecular Entity Capable of Improving Cognitive Function by Restoring the Phagocytic Aptitude of Microglia

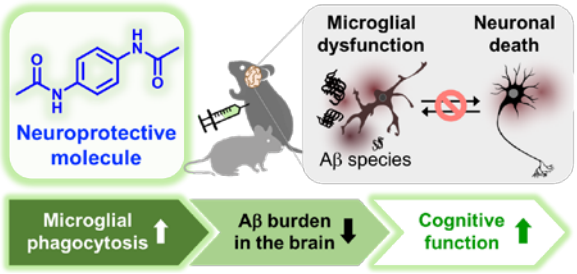

I thank Dr. Min Hee Park, Ju Youn Lee, Min Seock Jeong, Kang Ho Park, Seung Hoon Han, Professor Hee Kyung Jin, and Professor Jae-Sung Bae for *in vivo* studies employing APP/PS1 mice with data analysis; Mingeun Kim and Juhye Kang for characterization, gel/Western blot analysis, TEM, and cell studies; Geewoo Nam for writing; Eunyoung Tak, Min Sun Kim, and Professor Joo-Yong Lee for *in vivo* studies employing 5XFAD mice with data analysis. I carried out the preparation of reagents, gel/Western blot analysis, cell studies, analysis, organization of all data, and writing. I appreciate Professor Mi Hee Lim for her sincere dedication and guidance for me to complete this study.

ULSAN NATIONAL INSTITUTE OF SCIENCE AND TECHNOLOGY

1.1. Introduction

Neurodegeneration, defined as a progressive loss of neuronal structure and function, is the primary manifestation of many neurodegenerative diseases[1]. Increasing epidemiological evidence suggests that neuroinflammation, an innate immune mechanism of the central nervous system (CNS), is a major pathological contributor in neurodegeneration[2-5]. Microglia play a key role in this process, as they are the resident phagocytes in the CNS responsible for identifying and eliminating pathogens[2,6-12]. Under normal conditions, the microglial immune response balances opposing roles in which they can either excrete pro-inflammatory mediators, involved in cellular recruitment and removal of impaired neurons, or produce anti-inflammatory mediators, capable of promoting neuronal proliferation and synaptic plasticity[2,10,11]. In contrast, the persistent presence of pathologic triggers (*e.g.*, neuronal injury and protein aggregates) results in the chronic activation and impairment of microglia[2,7]. Microglial dysfunction is often characterized by (i) elevated expression of neurotoxic pro-inflammatory mediators; (ii) decreased production of neurotrophic anti-inflammatory mediators; (iii) compromised ability to remove pathogens through the loss of phagocytic capacity[2,7,9,10]. The combined effects of such microglial anomalies incite negative neuronal consequences[10], amplified through self-propagation and positive-feedback loops[2,7]. Therefore, microglial dysfunction is a potential target for drug discovery and may offer a therapeutic opportunity against neurodegenerative diseases, including Alzheimer's disease (AD)[2,7], Parkinson's disease[3], and amyotrophic lateral sclerosis[4].

AD is the most common form of dementia accounting for *ca.* 47 million cases in 2016, and the number of AD patients is projected to reach almost 131 million by 2050[13]. The multifaceted etiopathology of AD involves a variety of pathological factors, such as neuroinflammation and amyloidogenic proteins, including amyloid-β (Aβ)[14]. Moreover, the intertwined pathology between neuroinflammation and Aβ has been recognized to be critical towards the development of AD[7,15]. Loss of the phagocytic ability upon microglial dysfunction significantly decreases Aβ clearance and the subsequent elevation of Aβ levels can induce microglial impairment through chronic activation[2,9,16]. This malignant cycle is a strong driving force of neurodegeneration[17]. Thus, an efficient and effective strategy for restoring microglial function is necessary to reestablish neuronal homeostasis in AD.

Mounting research efforts have been dedicated to modulating microglial dysfunction with synthetic and repurposed chemical reagents[18-21]. Among the candidates, a synthetic NLRP3 (NACHT, LRR, and PYD domains-containing protein 3) inflammasome inhibitor, MCC950, exhibited restorative efficacy toward microglial dysfunction, promoting Aβ phagocytosis and improving cognitive function *in vivo*[22,23]. The aforementioned studies suggest that small molecules may be effective for regulating microglial dysfunction, but practical working examples are exceedingly rare. We report a novel neuroprotective compound, **1** (Figure 1.1a), as the smallest synthetic molecular entity capable of restoring cognitive defects to a significant extent by enhancing the microglial phagocytic clearance of Aβ aggregates in the brains of AD transgenic mice. We show that **1** downregulates the constituent

ULSAN NATIONAL INSTITUTE OF SCIENCE AND TECHNOLOGY

proteins of NLRP3 inflammasomes *in vivo* and subsequently lowers the production of the pro-inflammatory mediators, caspase-1 and IL-1β, leading to the recovery of microglial function. Our studies substantiate the possibility of designing small and simple molecules for rectifying microglial dysfunction and boosting microglial phagocytic aptitude. The new neuroprotective reagent, **1**, is a promising prototype of a remedial agent that can regulate neurodegenerative inflammation.

1.2. Results and Discussion

1.2.1. Design Rationale and Characterization of 1 as an Anti-Inflammatory Agent for Neuroprotection

A small molecule, **1** (Figure 1.1a), was rationally chosen based on the molecular framework of acetaminophen, an antipyretic and analgesic drug with widely accepted clinical efficacy and safety[24,25]. Recent studies have increasingly supported acetaminophen's neuroprotective activity involving the modulation of inflammatory pathways, apart from its well-known biological properties[26-33]. Cellular and *in vivo* investigations utilizing diverse cell lines and cognitively impaired animals reported neuroprotection by acetaminophen through the downregulation of overexpressed pro-inflammatory markers[26-33]. Based on its anti-inflammatory effects, we selected acetaminophen as the structural basis for designing a small molecule capable of controlling neuroinflammation. To obtain a more robust molecular structure (**1**; Figure 1.1a) than acetaminophen, a simple and straightforward structural modification was implemented to preemptively account for its potential chemical and metabolic instability (*e.g.*, oxidative transformation)[34] by replacing the phenol moiety with an acetamide functionality (Figure 1.2).

Prior to *in vivo* evaluation, the bioapplicability of **1** was investigated by determining its cytotoxicity, microsomal stability, and blood-brain barrier (BBB) permeability. First, no significant toxicity was observed in murine Neuro-2a (N2a) neuroblastoma cells treated with **1** at concentrations up to 500 μM (Figure 1.1b). Second, the metabolic studies of **1** using human liver microsomes revealed its moderate metabolic stability [half-life ($t_{1/2}$) > 60 min; intrinsic clearance (Cl_{int}) = 3.9; Figure 1.1c]. Lastly, the presence of **1** in the brains of CD1 mice after oral administration (10 mg/kg) indicated its potential to cross the BBB (Figure 1.1d). Together, **1** is determined to be suitable for *in vivo* assessment of its neuroprotective activity (*vide infra*).

ULSAN NATIONAL INSTITUTE OF SCIENCE AND TECHNOLOGY

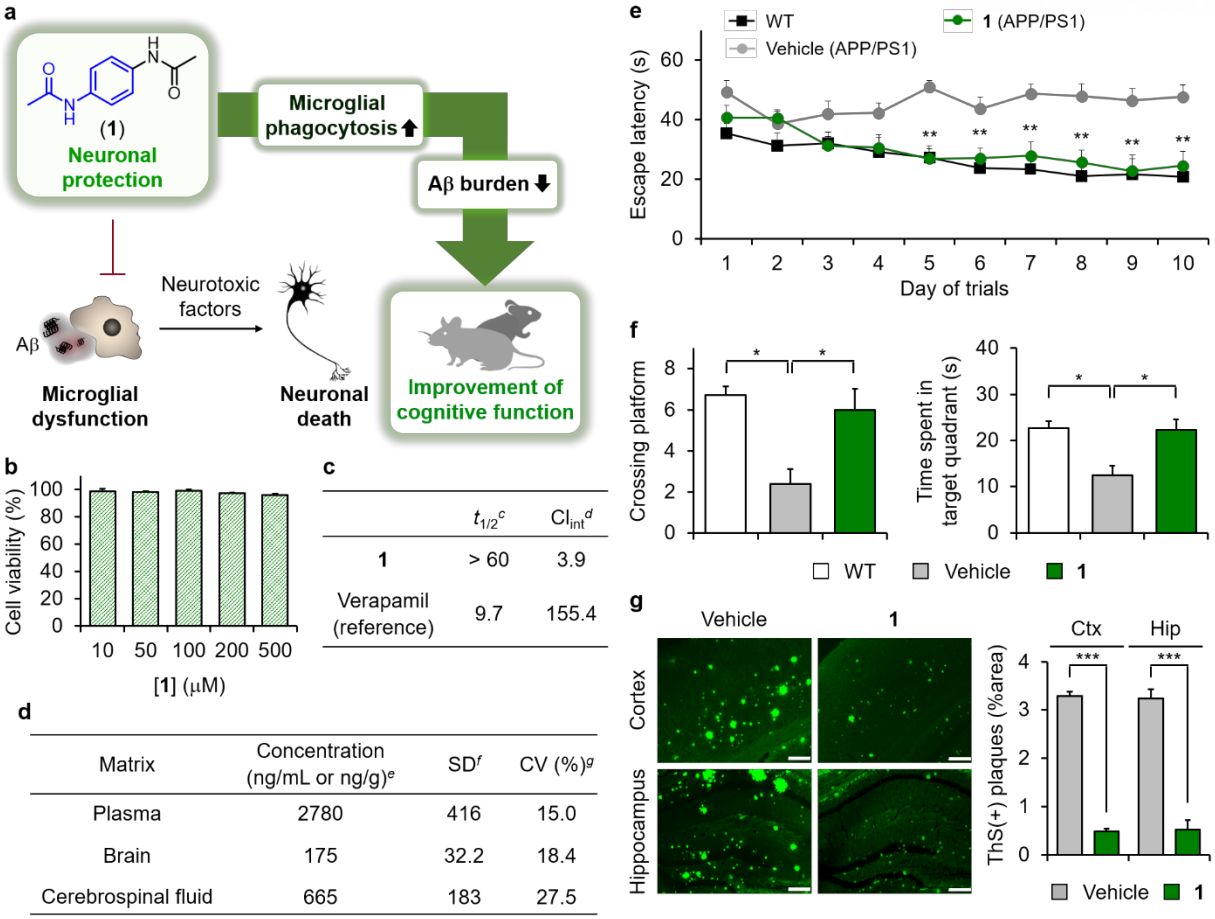

	$t_{1/2}$[c]	CL_{int}[d]
1	> 60	3.9
Verapamil (reference)	9.7	155.4

Matrix	Concentration (ng/mL or ng/g)[e]	SD[f]	CV (%)[g]
Plasma	2780	416	15.0
Brain	175	32.2	18.4
Cerebrospinal fluid	665	183	27.5

Figure 1.1. Overview of the studies presented in this work and *in vivo* efficacies of *N,N'-p*-phenylenebisacetamide (**1**). (a) Design, chemical structure, and working principle of **1** for *in vivo* efficacies. (b) Cytotoxicity of **1**. Cell viability (%) of N2a neuroblastoma cells incubated with various concentrations of **1** for 24 h was measured by the MTT assay [MTT = 3-(4,5-dimethylthiazol-2-yl)-2,5-diphenyltetrazolium bromide]. The cell viability (%) was calculated relative to cells treated with an equivalent amount of DMSO 1% v/v). The bars indicate the standard error from triplicate experiments. (c) Metabolic stability[a] and (d) brain uptake[b] of **1**. [a]Human liver microsomes; [b]CD1 mice; 10 mg/kg; per os, *p.o.*; 5 min administration; [c]half-life ($t_{1/2}$); [d]intrinsic clearance (CL_{int}); [e]mean (n = 3); [f]standard deviation; [g]coefficient of variation. (e) Escape latency time of vehicle- or **1**-treated APP/PS1 mice (vehicle or **1**) and wild-type mice (WT) in the Morris Water Maze (MWM) test. (f) Measurements of the crossing frequency and the time spend in target quadrant in the probe test. (g) Analysis of the amounts of Aβ plaques, detected by thioflavin-S (ThS), after the daily treatments of **1** for 2 months (2 mg/kg/day; intraperitoneal, *i.p.*) in APP/PS1 mice starting at 7.5 months of age. Scale bars = 200 μm. All data analysis was done at 9.5 months of age. Animal number: (e and f) n = 10 for WT mice or vehicle-treated APP/PS1 mice and n = 10 for **1**-treated APP/PS1 mice. (g) n = 4 for vehicle-treated or **1**-treated APP/PS1 mice. **P* < 0.05; ***P* < 0.01; ****P* < 0.001 by Student's *t* test or One-way analysis of variance, Tukey's post hoc test. All error bars indicate standard errors of mean (s.e.m.).

ULSAN NATIONAL INSTITUTE OF SCIENCE AND TECHNOLOGY

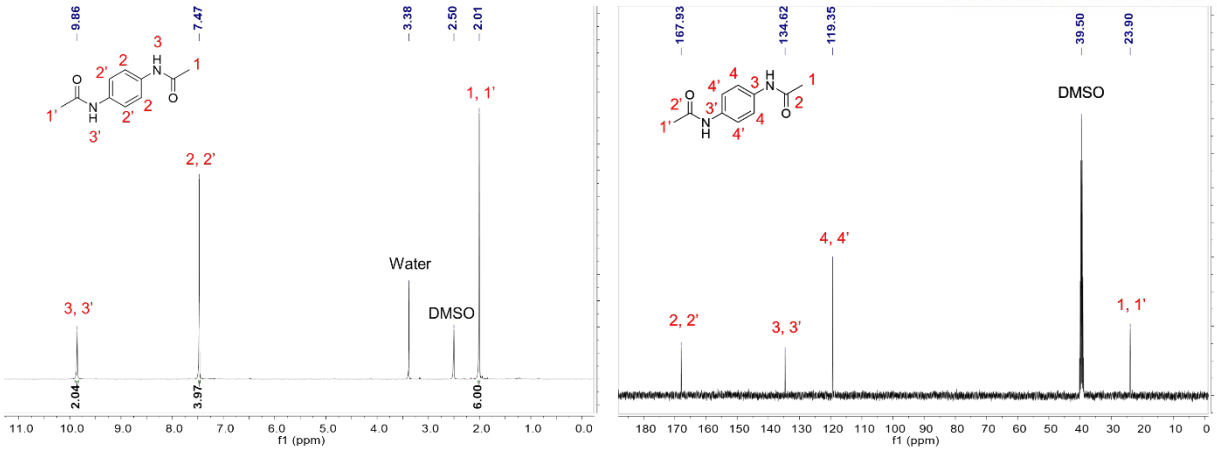

Figure 1.2. ^{1}H (400 MHz) and ^{13}C (100 MHz) NMR Spectra of **1** in DMSO-d_6.

1.2.2. 1 Improves Cognitive Deficits in AD Transgenic Mice with Reduced Amounts of Aβ Species

In vivo efficacy of **1** was first evaluated in APP/PS1 mice, an AD double transgenic mouse model that contains both mutant *amyloid precursor protein (APP)* and *presenilin-1 (PS1)* transgenes, characterized by increased production and accumulation of Aβ aggregates as well as notable cognitive impairment[35]. APP/PS1 mice (7.5 months of age) were subject to intraperitoneal (*i.p.*) administration of **1** or vehicle at 2 mg/kg/day for 2 months. After 30 days of treatment, the Morris Water Maze (MWM) test was carried out to examine the spatial learning and memory of wild-type (WT) and vehicle- or **1**-treated APP/PS1 mice. As shown in Figure 1.1e, the vehicle-treated APP/PS1 mice, relative to WT mice, exhibited noticeably longer escape latencies, while **1**-added APP/PS1 mice were able to locate the escape platform at time points comparable to those of WT mice. Such differences were especially notable from the 5th day of trials, at which point the escape latencies of vehicle- and **1**-treated APP/PS1 mice deviated by *ca.* 2-fold. In the probe trials conducted after 10 days of training, **1**-administered APP/PS1 mice traversed the target location more frequently and stayed in the objective quadrant for longer periods compared to APP/PS1 mice injected with vehicle (Figure 1.1f). Interestingly, **1**-treated APP/PS1 mice demonstrated similar results to WT mice, suggesting the restoration of spatial cognition. In the case of the locomotion and spontaneous activity of APP/PS1 mice, **1** did not induce significant changes in the fear conditioning, open field, and light and dark tests (Figure 1.3).

ULSAN NATIONAL INSTITUTE OF SCIENCE AND TECHNOLOGY

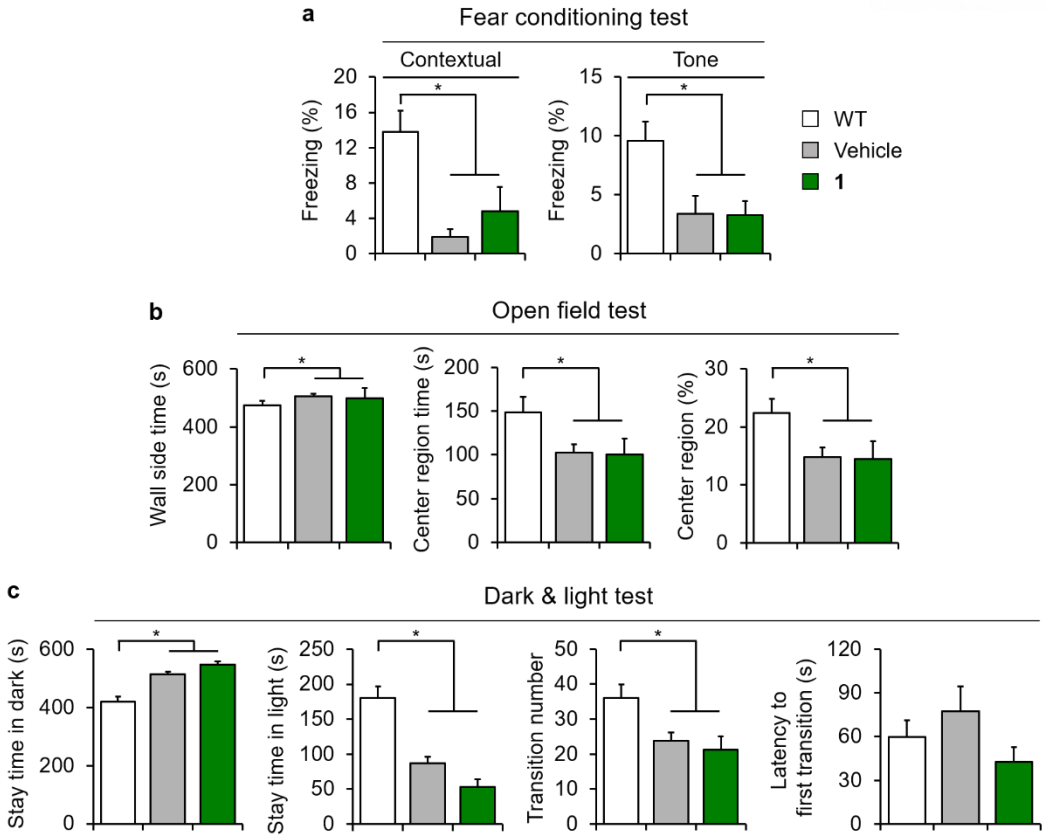

Figure 1.3. Behavioral tests of **1**-treated APP/PS1 mice (**1**; 2 mg/kg/day; *i.p.*) compared to wild-type mice (WT) and vehicle-added APP/PS1 mice (vehicle). (a) Fearing conditioning test. (b) Open field test. (c) Light and dark test. **1**-treated APP/PS1 mice (**1**). All data analysis was done at 9.5 months of age. Animal number: n = 10 for WT or vehicle-treated APP/PS1 mice; n = 10 for **1**-treated APP/PS1 mice. **P* < 0.05 by One-way analysis of variance, Tukey's post hoc test. The bars denote mean ± s.e.m.

The ability of **1** to restore cognitive function in AD transgenic mice was further confirmed employing 5XFAD mice, an AD transgenic mouse model overexpressing mutant human APP695 [K670N/M671L (Swedish), I716V (Florida), and V717I (London)] and PS1 (M146L and L286V) that indicates the rapid onset of AD pathology and behavioral decline[38-40]. In a fashion similar to APP/PS1 mice, 5XFAD mice treated with **1** (1 mg/kg/day; *i.p.*; 1 month; 4 months old) exhibited enhanced spatial learning and memory in the MWM test (Figure 1.4a and b). Moreover, the % area of 4G8-immunoreactive amyloid plaques was diminished in the brains of **1**-treated 5XFAD mice by *ca.* 40% compared to those of the vehicle-treated group (Figure 1.4c). In addition, the total, soluble, and insoluble levels of $A\beta_{40}$ were lowered by *ca.* 40%, 20%, and 50%, respectively (as for $A\beta_{42}$, *ca.* 30%, 35%, and 20% decreases were observed, respectively). Levels of soluble oligomeric Aβ, recognized as toxic Aβ species[41], were subject to a 30% reduction. The amount of congophilic amyloid plaques was also alleviated by 10%. Overall, our investigations with two AD transgenic mouse models demonstrate

ULSAN NATIONAL INSTITUTE OF SCIENCE AND TECHNOLOGY

that **1** can significantly improve cognitive defects and mitigate the accumulation of Aβ species (Figure 1.4d).

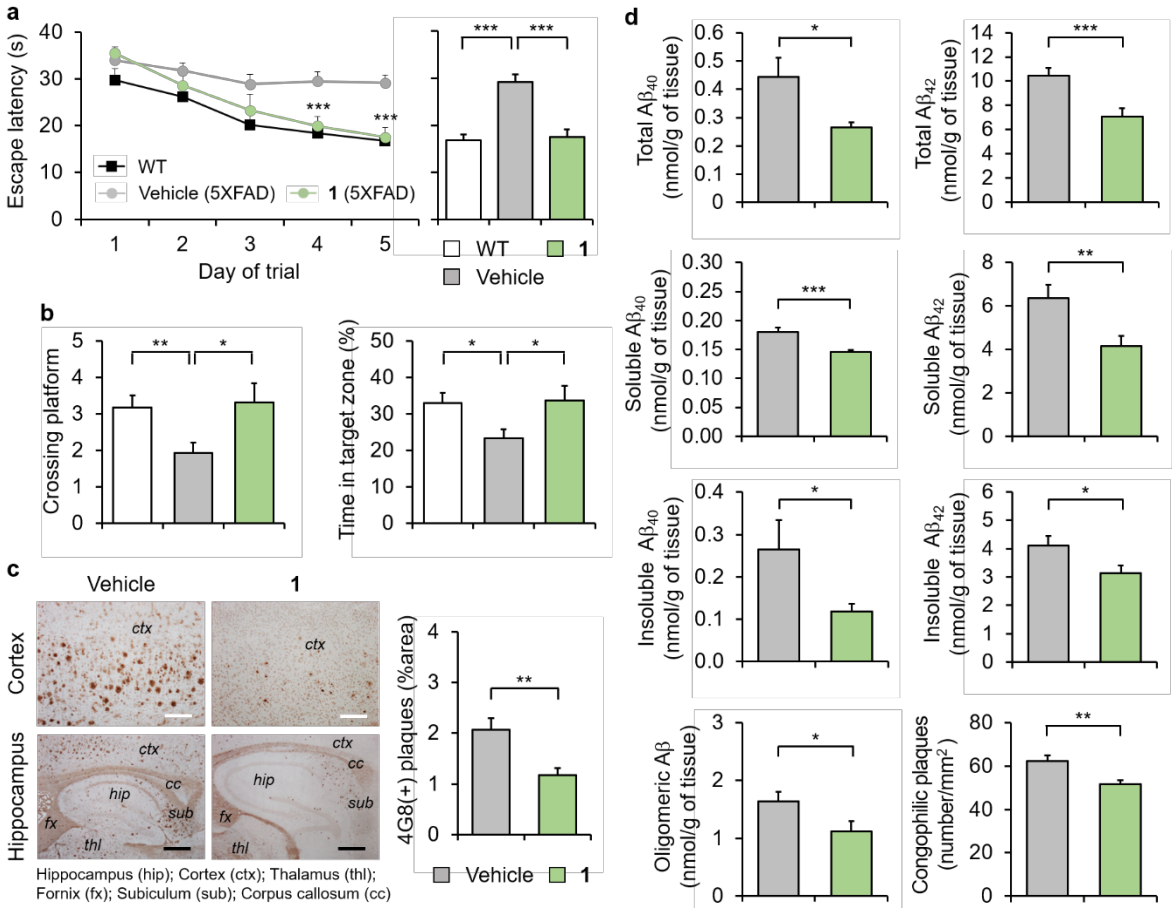

Figure 1.4. Efficacies of **1** on Aβ species and cognitive defects in 5XFAD mice after the daily treatment of **1** or vehicle for 1 month (1 mg/kg/day; *i.p.*) at 4 months of age. (a) Escape latency time of vehicle- or **1**-treated 5XFAD mice (vehicle or **1**) and WT in the Morris water maze test. (b) Measurements of the crossing frequency and the time spend in target quadrant in the probe test. (c) Analysis of the amounts of 4G8-immunoreactive amyloid deposits measured from the hippocampal (*hip*), cortical (*ctx*), and thalamic (*thl*) areas of the brain in vehicle- or **1**-treated 5XFAD mice (vehicle or **1**). Scale bars = 200 μm (white) and 500 μm (black). (d) Levels of total Aβ, soluble Aβ, insoluble Aβ, oligomeric Aβ and congophilic plaques in triplicate per sample. Animal number: (a and b) n = 17 for WT mice and n = 16 for vehicle- or **1**-treated 5XFAD mice; (c and d) n = 16 for each group. The bars denote mean ± s.e.m. **P* < 0.05; ***P* < 0.01; ****P* < 0.001 by unpaired *t*-test or ANOVA.

1.2.3. Administration of 1 in APP/PS1 Mice Attenuates Neuroinflammation

To determine whether the anti-inflammatory effects of **1** caused the decrease in the levels of Aβ species, microglia and astrocytes, the two major resident immune cells involved in the inflammatory response[2,7], were histologically monitored using anti-Iba1 and anti-GFAP antibodies[16] in the brains of APP/PS1 mice (2 mg/kg/day, *i.p.*; 2 months; 7.5 months old). As shown in Figure 1.5a and b, the increased glial

ULSAN NATIONAL INSTITUTE OF SCIENCE AND TECHNOLOGY

activation in APP/PS1 mice, induced by chronic neuroinflammation, was reduced by **1**. Activation of microglia in both the cortex and hippocampus was decreased by *ca.* 50% with the treatment of **1** compared to vehicle-added APP/PS1 mice (note that the activation of astrocyte was lowered by *ca.* 30%). In addition, the expression of pro-inflammatory markers (*i.e.*, TNF-α, IL-1β, IL-6, and iNOS)[16] and immunoregulatory cytokine (*i.e.*, IL-10)[16], elevated in vehicle-treated APP/PS1 mice, was declined to levels comparable to those of WT mice upon administration of **1** in APP/PS1 mice (Figure 1.5c). On the other hand, the amounts of anti-inflammatory markers (*i.e.*, IL-4, TGF-β, and Arg1)[16], downregulated in APP/PS1 mice introduced with vehicle, were enhanced in the **1**-treated group. Therefore, our histological and biochemical experiments support that **1** is able to lower the chronic activation of microglia and astrocytes under neuroinflammatory conditions.

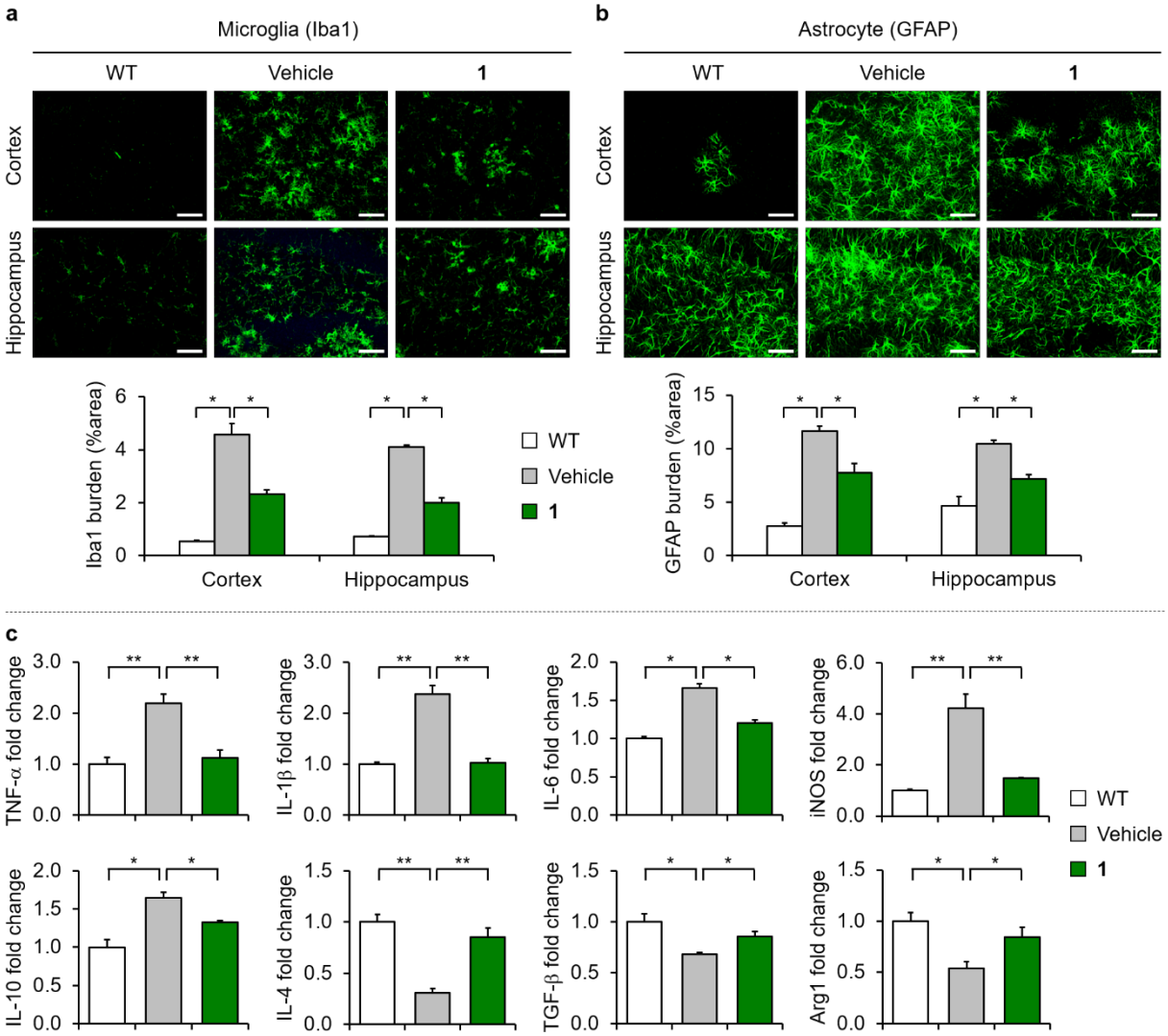

Figure 1.5. Change in neuroinflammation upon treatment of **1** in wild-type (WT) and APP/PS1 mice. (a and b) Representative images and quantification of activated microglia (Iba1) and astrocyte (GFAP). Scale bars = 50 μm (c) Analysis of alteration in mRNA levels of pro- and anti-inflammatory cytokines after administration of **1** into WT mice (WT), vehicle-treated APP/PS1 mice (vehicle), and **1**-treated

ULSAN NATIONAL INSTITUTE OF SCIENCE AND TECHNOLOGY

APP/PS1 mice (**1**). Pro-inflammatory marker: TNF-α, IL-1β, IL-6, and iNOS, Immunoregulatory cytokine: IL-10, Anti-inflammatory marker: IL-4, TGF-β, and Arg1. All data analysis was done at 9.5 months of age. Animal number: (a-c) n = 4 for WT mice and n = 4 for vehicle- or **1**-treated APP/PS1 mice. $*P < 0.05$; $**P < 0.01$ by One-way analysis of variance, Tukey's post hoc test. All error bars indicate s.e.m.

1.2.4. Anti-Neuroinflammatory Effects of 1 Originate from Microglia

To identify the cellular source of **1**'s anti-inflammatory activity, Aβ-induced alterations in the *in vitro* expression of inflammatory markers were first examined in three types of brain cells (*i.e.*, microglia, astrocytes, and neurons) with and without the treatment of **1**. The conditioned media (CM), containing a secreted mixture of diverse signaling mediators[42], from these three types of cells were collected and treated to either astrocytes (CM from microglia) or microglia (CM from astrocytes or neurons). In the presence of $A\beta_{42}$ (Figure 1.6a, top), microglia exhibited elevated levels of pro-inflammatory markers (*i.e.*, TNF-α, IL-1β, IL-6, and iNOS)[16] and immunoregulatory cytokine (*i.e.*, IL-10)[16], as well as reduced amounts of anti-inflammatory markers (*i.e.*, IL-4, TGF-β, and Arg1)[16], relative to the control (*i.e.*, microglia without $A\beta_{42}$ incubation). The concurrent introduction of **1** and $A\beta_{42}$ to microglia could noticeably restore the expression of inflammatory markers to the levels comparable to those of the control (Figure 1.6a, top), indicating that **1** mitigated the Aβ-mediated inflammatory response in microglia. The CM from Aβ-treated microglia triggered an inflammatory response in astrocytes, evidenced by the changes in the expression of inflammatory markers (Figure 1.6a, bottom). Astrocytes incubated in the CM from **1**-treated microglia expressed inflammatory markers at the levels comparable to those of the astrocytes incubated with the CM from the control group.

In contrast, the direct treatment of **1** did not abate the Aβ-triggered inflammatory response in astrocytes (Figure 1.6b, top). The CM from astrocytes incubated with $A\beta_{42}$ and **1** induced an inflammatory response in microglia (Figure 1.6b, bottom), suggesting that **1** could not divert the astrocyte-mediated modulation of inflammatory signaling in microglia. Moreover, **1** could not prevent Aβ-induced changes in the expression of neuronal 'off' signals (*i.e.*, BDNF, CD47, and CD200) and a majority of the 'on' signals (*i.e.*, CXCL10 and CCL21) (Figure 1.6c, top), responsible for sustaining the resting state and eliciting the activation of microglia, respectively[16,43]. Similar to the CM from Aβ-treated neurons, the CM from **1**-added neurons provoked an inflammatory response in microglia (Figure 1.6c, bottom). Together, these observations indicate that **1** is capable of directly diminishing the Aβ-induced inflammatory response of microglia among the three types of cells tested in this study. Moreover, through indirect effects prompted by microglia, **1** may be able to prevent the secondary inflammatory response in astrocytes. Thus, the anti-inflammatory effects of **1** could stem from its direct influence against microglia, responsible for the propagation of inflammatory signaling.

ULSAN NATIONAL INSTITUTE OF SCIENCE AND TECHNOLOGY

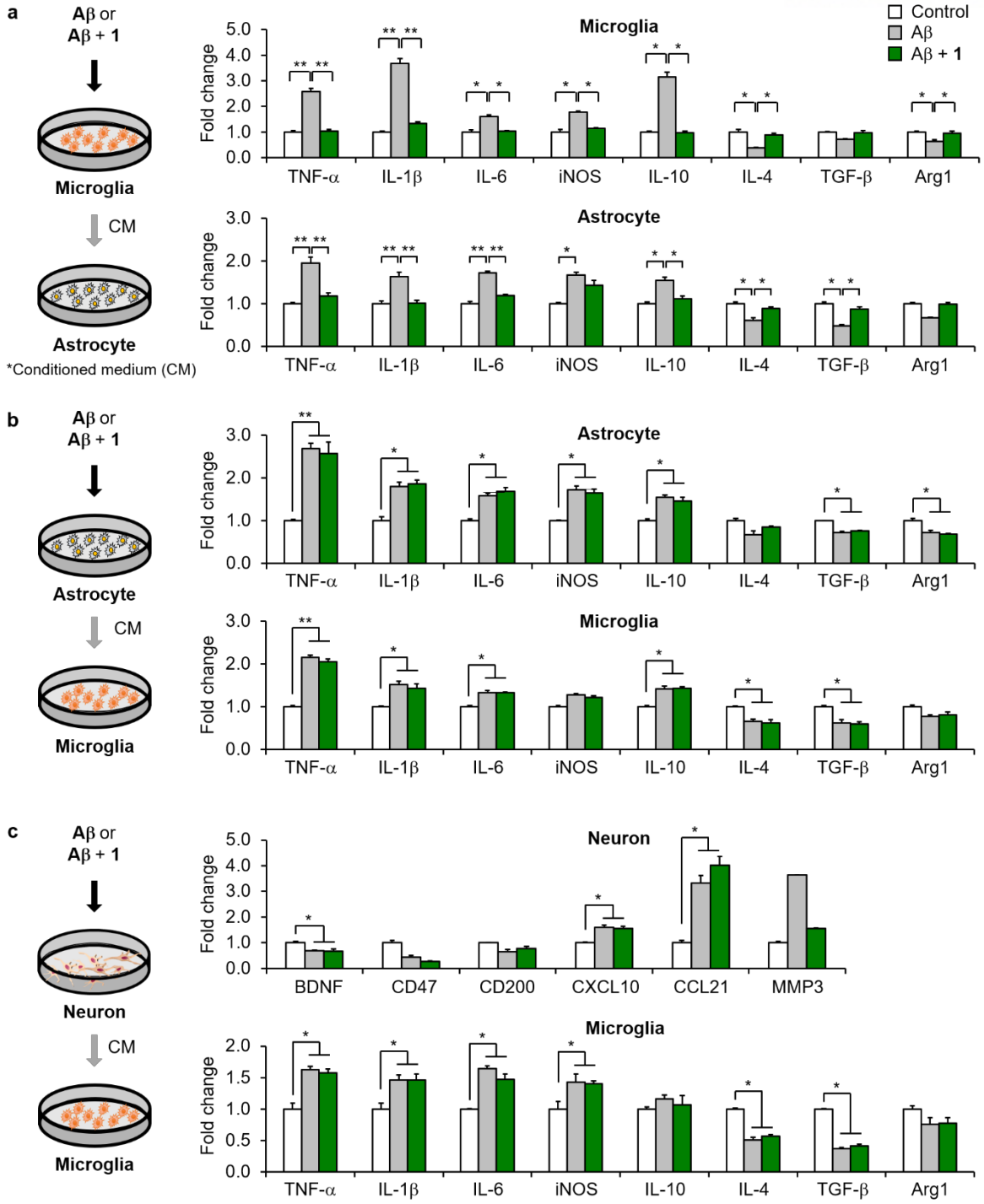

Figure 1.6. Identification of the responsible cells upon incubation of $A\beta_{42}$ with and without **1**. (a) Analysis of mRNA levels of inflammatory cytokines in microglia by treatment of $A\beta_{42}$ species with and without **1** or in astrocytes [grown by transferring the conditioned media (CM) harvested from the microglia] (n = 3 independent experiments). (b) Measurement of mRNA levels of inflammatory cytokines in astrocytes upon addtion of $A\beta_{42}$ species with and without **1** or in microglia (grown by transferring the CM harvested from the astrocytes) (n = 3 independent experiments). (**c**) Determination of mRNA levels of off/on signals in neurons with incubation of $A\beta_{42}$ species with and without **1** or inflammatory cytokines in microglia (grown by transferring the CM harvested from the neurons) (n = 3 independent experiments). Conditions: [$A\beta_{42}$] = 10 μM; [**1**] = 10 μM; pro-inflammatory marker: TNF-

ULSAN NATIONAL INSTITUTE OF SCIENCE AND TECHNOLOGY

α, IL-1β, IL-6, and iNOS; immunoregulatory cytokine: IL-10; anti-inflammatory marker: IL-4, TGF-β, and Arg1; off signals*:* BDNF, CD4, and CD200; on signals: CXCL10, CCL21, and MMP3. **P* < 0.05; ***P* < 0.01 by One-way analysis of variance, Tukey's post hoc test. All error bars indicate s.e.m.

Table 1.1. Sequences of primer pairs.

Gene[a]	Forward	Reverse
TNF-α	5'-GATTATGGCTCAGGGTCCAA-3'	5'-GCTCCAGTGAATTCGGAAAG-3'
IL-1β	5'-CCCAAGCAATACCCAAAGAA-3'	5'-GCTTGTGCTCTGCTTGTGAG-3'
IL-6	5'-CCGGAGAGGAGACTTCACAG-3'	5'-TTGCCATTGCACAACTCTTT-3'
iNOS	5'-CACCTGGAACAGCACTCTCT-3'	5'-CTTTGTGCGAAGTGTCAGTG-3'
IL-10	5'-AAGGCCATGAATGAATTTGA-3'	5'-TTCGGAGAGAGGTACAAACG-3'
IL-4	5'-ATCCATTTGCATGATGCTCT-3'	5'-GAGCTGCAGAGACTCTTTCG-3'
TGF-β	5'-TTACCTGGATGGAAGTGGAA-3'	5'-TGTTATGAGGAAGGGGACAA-3'
Arg1	5'-AAGCCAAGGTTAAAGCCACT-3'	5'-CGATTCACCTGAGCTTTGAT-3'
CXCL10	5'-AAAAGGGCTCCTTAACTGGA-3'	5'-GCTGGTCACCTTTCAGAAGA-3'
CCL21	5'-AGCTATGTGCAAACCCTGAG-3'	5'-CTCTTGAGGGCTGTGTCTGT-3'
MMP3	5'-GGGTAGGATGAGCACACAAC-3'	5'-TAGAAGGAGGCAGCAGAGAA-3'
CD47	5'-TGGTATCCAGCAAGCCTTAG-3'	5'-AAGACACCAGTGCCATCAAT-3'
BDNF	5'-AATTTGGTAAACGGCACAAA -3'	5'-GCAAACAATCGCTTCATCTT-3'
CD200	5'-CAGGAACCCTTGATTGTGAC -3'	5'-AGTTCCAGAGTCCCAGCTCT-3'
NEP	5'-GAAATTCAGCCAAAGCAAGC-3'	5'-GATTTCGGCCTGAGGAATAA-3'
MMP9	5'-CCATGTCACTTTCCCTTCAC-3'	5'-CTCACTAGGGCAGAAACCAA-3'
IDE	5'-GAAGACAAACGGGAATACCGTG-3'	5'-CCGCTGAGGACTTGTCTGTG-3'
GAPDH	5'-TGAATACGGCTACAGCAACA-3'	5'-AGGCCCCTCCTGTTATTATG-3'

[a]TNF-α, tumor necrosis factor-alpha; IL-1β, interleukin-1β; IL-6, interleukin-6; iNOS, inducible nitric oxide synthase; IL-10, interleukin-10; IL-4, interleukin-4; TGF-β, transforming growth factor-β; Arg1, arginase 1; CXCL10, chemokine (C-X-C Motif) ligand 10; CCL21, chemokine (C-C Motif) ligand 21; MMP3, matrix metallopeptidase 3; CD47, cluster of differentiation 47; BDNF, brain-derived neurotrophic factor; CD200, cluster of differentiation 200; NEP, neprilysin; MMP9, matrix metallopeptidase 9; IDE, insulin degrading enzyme; GAPDH, glyceraldehyde 3-phosphate dehydrogenase.

1.2.5. 1 Promotes the Phagocytic Capacity of Microglia under Chronic Neuroinflammation

The phagocytic capability of microglia poses an important aspect of the inflammatory response against external stimuli, such as Aβ, the persistent presence of which can induce chronic microglial activation[2,7]. With confirmation that the anti-inflammatory activity of the molecule originates from microglia (Figure 1.6), the influence of **1** towards microglial phagocytosis, defective under AD-related pathological conditions[7,16], was analyzed *in vivo* using confocal microscopy. Volumetric quantification of the

ULSAN NATIONAL INSTITUTE OF SCIENCE AND TECHNOLOGY

overlapping fluorescence regions through 3D reconstruction conferred a numerical representation of the microglial phagocytic process.

Images of the brain slices co-immunostained with an anti-Iba1 antibody[16] and ThS[37] showed that Aβ-associated microglial recruitment was increased in **1**-treated APP/PS1 mice (2 mg/kg/day, *i.p.*; 2 months; 7.5 months old) compared to vehicle-treated APP/PS1 mice (Figure 1.7a). In order to examine the phagocytic aptitude of microglia more closely, Lamp1, a membrane protein expressed in microglial lysosomes[16,44], was monitored, along with Iba1- and ThS-reactive amyloid plaques. Overlaying regions of the three fluorescence images presented the formation and location of Aβ-associated phagolysosomes, indicating the ongoing microglial phagocytosis of Aβ[16,44] (Figure 1.7b). The treatment of **1** in APP/PS1 mice increased the volumes of microglial phagolysosomes, Aβ-associated phagolysosomes, and microglia occupied by Aβ-loaded phagolysosomes by *ca.* 2.8, 1.3 and 2.3-fold, respectively, relative to those of vehicle-treated APP/PS1 mice (Figure 1.7b, bottom).

Additionally, the morphology of microglia, closely related to its function[16,45], was analyzed to confirm the effects of **1** on the phagocytic function of microglia. The amoeboid morphology of Aβ-associated microglia in **1**-treated APP/PS1 mice indicated that the compound could enhance the microglial phagocytosis of Aβ (Figure 1.7c). Quantification of the morphological parameters confirmed the transition of **1**-incubated microglia towards its phagocytic state: treatment of **1** decreased microglial volume, dendrite length, and number of segments, terminal points, and branch points and increased cell body size (Figure 1.7c, bottom). Lastly, **1**-administrated APP/PS1 mice exhibited increased levels of smaller Aβ species (< 25 μm) and decreased amounts of larger Aβ aggregates (25-50 μm, > 50 μm), compared to those of the vehicle-treated APP/PS1 mice (Figure 1.7d). Therefore, it can be inferred that the enhanced phagocytic capacity of **1**-treated microglia led to an increase in the degradation of larger Aβ species. Overall, our immunohistological studies demonstrate that **1** can restore the phagocytic activity of microglia, defective in APP/PS1 mice[16,46], evidenced by the increased co-localization of Aβ plaques and lysosomes within microglia, shifts in microglial morphology, and changes in the size distribution of Aβ aggregates.

ULSAN NATIONAL INSTITUTE OF SCIENCE AND TECHNOLOGY

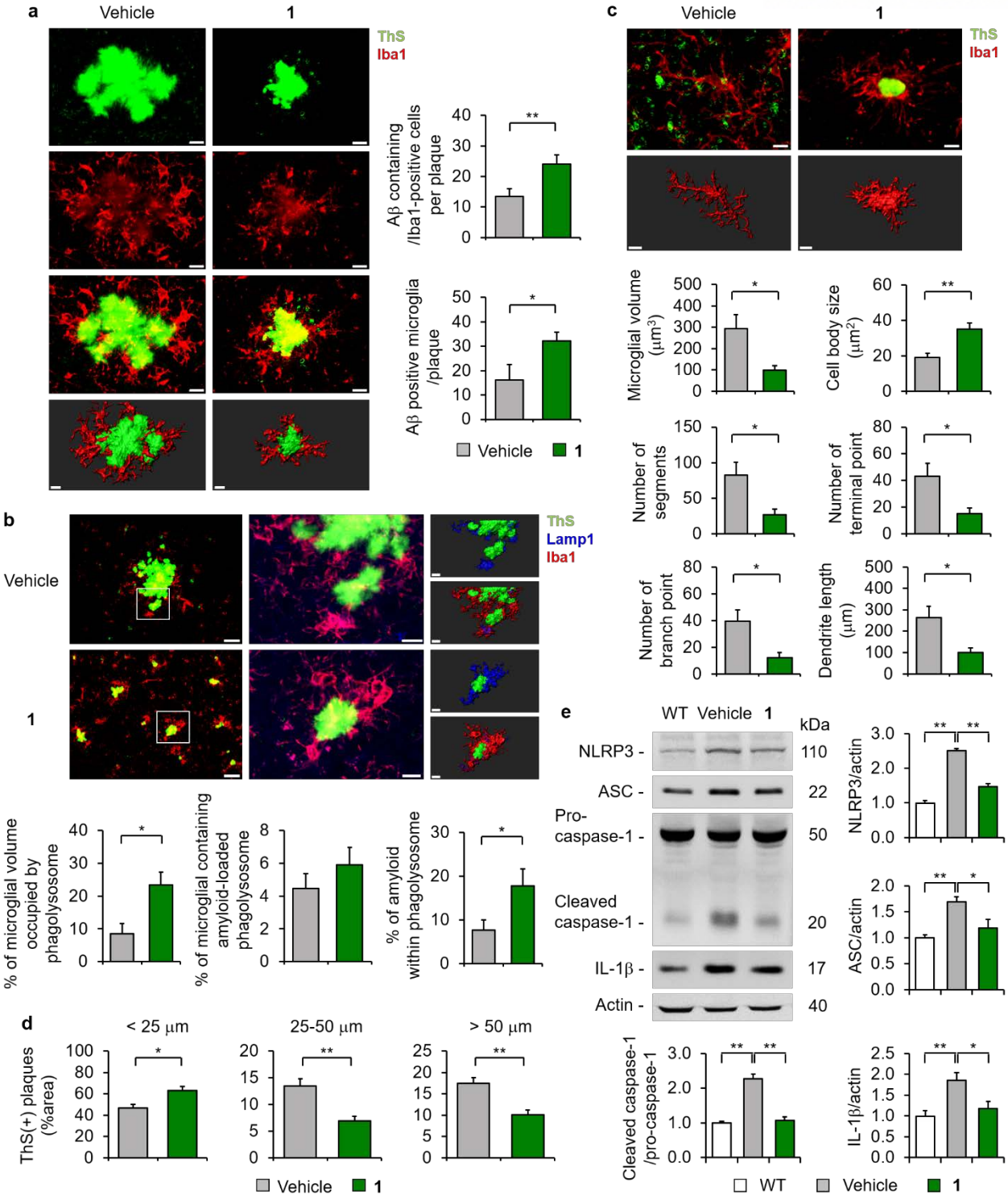

Figure 1.7. Analysis of the microglial phagocytosis of Aβ and the activity of NLRP3 inflammasome-related proteins in **1**-treated APP/PS1 mice. (a) Colocalization of the microglia (Iba1, red) with Aβ aggregates (ThS, green) and quantification. Scale bars = 10 μm. 3D reconstruction from confocal image stacks. Scale bars = 10 μm. (b) Immunofluorescence images of Aβ aggregates (ThS, green) encapsulated within phagolysosome (Lamp1, blue) in microglia (Iba1, red) in the brains of vehicle- or **1**-treated APP/PS1 mice. Quantification of the microglial volume occupied by Lamp1(+) phagolysosomes, percent of the microglia containing Aβ-loaded phagolysosome, and Aβ encapsulated

ULSAN NATIONAL INSTITUTE OF SCIENCE AND TECHNOLOGY

in phagolysosomes. Low magnification scale bars = 40 μm; high magnification scale bars = 10 μm. 3D reconstruction from confocal image stacks. Scale bars = 10 μm. (c) Morphology of microglia (Iba1, red) surrounding Aβ (ThS, green) in the cortex of vehicle- or **1**-treated APP/PS1 mice. Scale bars = 10 μm. 3D reconstruction from confocal image stacks. (d) Morphometric analysis of Aβ plaques in vehicle- or **1**-treated APP/PS1 mice. (e) Effects of **1** on the activity of NLRP3 inflammasome-related proteins. Wild-type mice (WT), vehicle-treated APP/PS1 mice (vehicle), and **1**-treated APP/PS1 mice (**1**). All data analysis was done at 9.5 months of age. Animal number: (a-d) n = 3 for vehicle- or **1**-treated APP/PS1 mice; (e) n = 4 for WT mice and n = 4 for vehicle-treated or **1**-treated APP/PS1 mice. $*P < 0.05$; $**P < 0.01$ by Student's t test or One-way analysis of variance, Tukey's post hoc test. All error bars indicate s.e.m.

1.2.6. 1 Downregulates the Constituent Proteins of NLRP3 Inflammasomes

The NLRP3 inflammasome is a signaling mediator composed of NLRP3, ASC (apoptosis-associated speck-like protein containing CARD), and pro-caspase-1[22,47]. Activated NLRP3 inflammasomes are responsible for cleaving pro-caspase-1 to produce caspase-1, which subsequently promotes the maturation of IL-1β, a representative pro-inflammatory cytokine[47]. Thus, the inhibition of NLRP3 inflammasome activity has received attention as a promising strategy to diminish neuroinflammation in AD[22,47]. Previous research reported that acetaminophen suppressed the NLRP3 inflammasome pathway under pathological conditions[48]. To further comprehend **1**'s anti-inflammatory activity, its influence on the expression of NLRP3 inflammasome-associated proteins, *i.e.*, NLRP3, ASC, and IL-1β, in APP/PS1 mice was investigated by gel electrophoresis and Western blot (gel/Western blot). As presented in Figure 1.7e, **1** downregulated the production of NLRP3, ASC, and IL-1β. Moreover, a notable decrease in the ratio of cleaved caspase-1 to pro-caspase-1 was observed upon treatment of **1**. These results suggest that the suppressed generation of NLRP3 and ASC by **1** may reduce the activation of caspase-1 and consequently IL-1β. Therefore, **1** may intervene in an upstream process which regulates the expression of NLRP3 and ASC.

1.2.7. 1 Does Not Alter Aβ Aggregation and Aβ-Degrading Enzymes' Expression

To validate that the reduction of Aβ accumulation, observed in the brains of **1**-treated AD transgenic mice, was indeed a product of **1**'s anti-inflammatory activity over direct influence on a decrease in Aβ deposition, the modulating effects of the compound towards the aggregation pathways of $Aβ_{40}$ and $Aβ_{42}$, two major isoforms of Aβ[49], and the expression of Aβ-degrading enzymes were probed *in vitro* and *in vivo* (WT and APP/PS1 mice), respectively. First, the effects of **1** towards inhibition of Aβ aggregate formation [inhibition experiment, Figure 1.8a (i)] and disassembly of preformed Aβ aggregates [disaggregation experiment, Figure 1.8a (ii)] were assessed through gel/Western blot and transmission electron microscopy (TEM). In both inhibition and disaggregation experiments, the Aβ species resulted from incubation with **1** did not exhibit noticeable changes in the size distribution and morphology,

ULSAN NATIONAL INSTITUTE OF SCIENCE AND TECHNOLOGY

relative to those generated without **1** (Figure 1.8b and c). In short, **1** does not modify the aggregation pathways of both $A\beta_{40}$ and $A\beta_{42}$.

Moreover, the expression of enzymes responsible for Aβ degradation [*i.e.*, neprilysin (NEP), matrix metallopeptidase 9 (MMP9), and insulin-degrading enzyme (IDE)] was analyzed in the brain samples of WT and vehicle- or **1**-treated APP/PS1 mice. As depicted in Figure 1.8d, vehicle-treated APP/PS1 mice, compared to WT mice, indicated the reduced levels of NEP, MMP-9, and IDE, even with the administration of **1** (2 mg/kg/day, *i.p.*; 2 months; 7.5 months old). These observations indicate that **1** has no effect on the production of Aβ-degrading enzymes. Thus, our studies suggest the restored microglial phagocytic capacity *via* the treatment of **1** as the dominant to be responsible for alleviating the accumulation of Aβ species in the brains of AD transgenic mice.

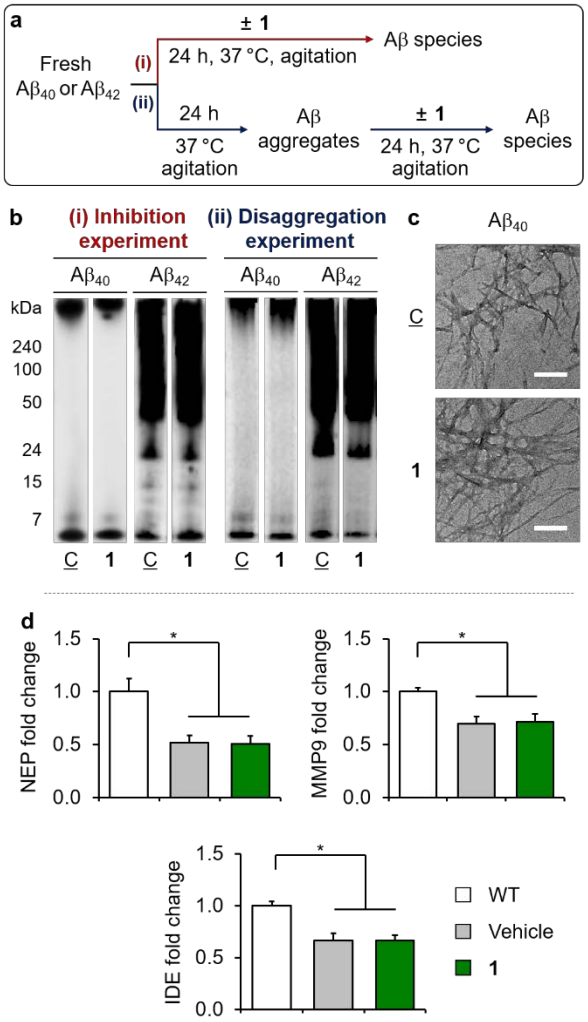

Figure 1.8. Effects of **1** on the aggregation of Aβ and the expression of Aβ-degrading enzymes. (a) Scheme of the (i) inhibition and (ii) disaggregation experiments. (b) Visualization of the size distribution of the resultant $A\beta_{40}$ and $A\beta_{42}$ species from (i) and (ii) by gel/Western blot using an anti-Aβ antibody (6E10). Lanes: (C) $A\beta_{40}$ or $A\beta_{42}$; (**1**) $A\beta_{40}$ or $A\beta_{42}$ + **1**. (c) TEM images of the samples obtained from (b, i). Scale bars = 200 nm. Conditions: [$A\beta_{40}$ or $A\beta_{42}$] = 25 μM; [**1**] = 50 μM; 20 mM HEPES, pH 7.4,

ULSAN NATIONAL INSTITUTE OF SCIENCE AND TECHNOLOGY

150 mM NaCl; 24 h; 37 °C; constant agitation. (d) Analysis of the levels of the enzymes (*i.e.*, NEP, MMP9, and IDE) involved in Aβ degradation in wild-type mice (WT) and vehicle- or **1**-administrated APP/PS1 mice (vehicle or **1**). All data analysis was done at 9.5 months of age. Animal number: (d) n = 4 for WT mice and n = 4 for vehicle- or **1**-treated APP/PS1 mice. **P* < 0.05 by One-way analysis of variance, Tukey's post hoc test. All error bars indicate s.e.m.

1.3. Conclusion

Dysfunction of microglia, a pivotal mediator of neuroinflammation, has been increasingly recognized as a causative factor in AD[2]; thus, developing chemical reagents capable of restoring microglial function is critically important and constitutes a promising but underexplored therapeutic strategy. We report that **1** is the smallest synthetic neuroprotective agent known to date with the ability to promote microglial phagocytic function. The activity of **1** leads to effective attenuation of cognitive deficits in two types of AD transgenic mice (*i.e.*, APP/PS1 and 5XFAD mice) and noticeable reduction of Aβ accumulation. Downregulation of the constituent proteins of NLRP3 inflammasomes (*i.e.*, NLRP3 and ASC), witnessed in the brains of APP/PS1 mice administrated with **1**, is most likely responsible for the rescue from microglial dysfunction. Our studies suggest that disrupting the malign neuroinflammatory cycle can improve cognitive impairment found in the AD-affected brain. Therefore, more specific approaches to regulate neuroinflammation in AD through the rectification of microglial dysfunction using small molecules are confirmed as a valid therapeutic approach against AD. Furthermore, neuroprotective small molecules capable of recovering microglial dysfunction with subsequent elevation of microglial phagocytic function could also serve as investigative tools to advance our understanding of the role of neuroinflammation in AD pathology.

1.4. Experimental Section

1.4.1. Materials and Methods

All chemical reagents were purchased from commercial suppliers and used as received unless otherwise stated. Compound **1** was purchased from Alfa Aesar (Ward Hill, MA, USA) and characterized by a Bruker AVHD400 NMR spectroscopy [Korea Advanced Institute of Science and Technology (KAIST) Analysis center for Research Advancement (KARA), KAIST, Daejeon, Republic of Korea] and a micrOTOF-Q II mass spectrometer (HRMS; KARA). $A\beta_{40}$ (DAEFRHDSG-YEVHHQKLVFFAEDVGSNKGAIIGLMVGGVV) and $A\beta_{42}$ (DAEFRHDSGYEVHHQKLVFFAED-VGSNKGAIIGLMVGGVVIA) were purchased from Anaspec (Fremont, CA, USA). HEPES [*N*-(2-hydroxyethyl)piperazine-*N*′-(2-ethanesulfonic acid)] was purchased from Sigma-Aldrich (St. Louis, MO, USA). The buffered solution was prepared in doubly distilled water [ddH_2O; a Milli-Q Direct 16 system (18.2 MΩ·cm; Merck KGaA, Darmstadt, Germany)]. Trace metal contamination was removed from the solutions used for the experiments by treating with Chelex (Sigma-Aldrich) overnight. The

ULSAN NATIONAL INSTITUTE OF SCIENCE AND TECHNOLOGY

absorbance in cell viability studies was measured by a SpectraMax M5e microplate reader (Molecular Devices, Sunnyvale, CA, USA). Metabolic stability assay to predict the half-life and clearance of compounds was evaluated with human liver microsomes [Daegu Gyeongbuk Medical Innovation Foundation (DGMIF), Daegu, Republic of Korea]. Analysis of the brain uptake of **1** in male CD1 mice was implemented at Shanghai ChemPartner (Shanghai, China). The concentration of Aβ was determined by an Agilent 8453 UV–Vis spectrophotometer (Santa Clara, CA, USA). The gel images were recorded on a ChemiDoc MP Imaging System (Bio-Rad, Hercules, CA, USA). Transmission electron microscopical images were obtained by a JEOL JEM-2100 transmission electron microscope [Ulsan National Institute of Science and Technology (UNIST) Central Research Facilities (UCRF), UNIST, Ulsan, Republic of Korea].

1.4.2. Characterization of 1

^{1}H NMR [400 MHz, DMSO-d_6, δ(ppm)]: 9.86 (s, 2H), 7.47 (s, 4H), 2.01 (s, 6H). ^{13}C NMR [100 MHz, DMSO-d_6, δ(ppm)]: 167.9, 134.6, 119.4, 23.9. HRMS: *m/z* Calcd for $C_{10}H_{12}N_2O_2$ $[M + H]^+$: 193.0972; found: 193.0980.

1.4.3. Cell Viability Studies

The murine neuroblastoma Neuro-2a (N2a) cell line [American Type Cell Collection (ATCC), Manassas, VA, USA] was maintained in media containing 1:1 DMEM (GIBCO, Grand Island, NY) and opti-MEM (GIBCO), 5% (v/v) fetal bovine serum (FBS; Sigma-Aldrich), and 100 U/mL penicillin and 100 mg/mL streptomycin (GIBCO). The N2a cells were grown and maintained at 37 °C in a humidified atmosphere with 5% CO_2. Cell viability upon treatment with **1** was determined by the MTT assay [MTT = 3-(4,5-dimethylthiazol-2-yl)-2,5-diphenyltetrazolium bromide]. The cells were seeded in a 96-well plate (10,000 cells in 100 μL per well). The cells were treated with **1** (10, 50, 100, 200, and 500 μM; 1% v/v final DMSO concentration) and incubated for 24 h. After incubation, MTT [25 μL; 5 mg/mL in phosphate buffered saline (PBS; pH 7.4)] was added to each well and the plate was incubated for 4 h at 37 °C. Formazan produced by the cells was solubilized using an acidic solution of *N*,*N*-dimethylformamide (DMF; 50% v/v, aq) and sodium dodecyl sulfate (SDS; 20% w/v) overnight at room temperature in the dark. The absorbance was measured at 600 nm by the microplate reader. Cell viability was calculated relative to cells containing an equivalent amount of DMSO.

1.4.4. Metabolic Stability Assay

1 (1 μM) was added into the PBS solution (0.1 M, pH 7.4) containing human liver microsomes (0.5 mg/mL), and was incubated for 5 min at 37 °C. Dihydronicotinamide adenine dinucleotide phosphate (NADPH) regeneration system solution was introduced to the pre-incubated mixture and then incubated for 15, 30, and 60 min at 37 °C. To terminate the reaction, the acetonitrile (CH_3CN) solution that

ULSAN NATIONAL INSTITUTE OF SCIENCE AND TECHNOLOGY

included chlorpropamide known as an internal standard was added. After a centrifugation (14,000 rpm, 4 °C) for 5 min, the supernatant was injected for the analysis of **1** and its possible metabolites into the LC-MS/MS system (DGMIF).

1.4.5. Brain Uptake Studies

After 5 min administration of **1** in male CD1 mice (10 mg/kg; per os, *p.o*), the mice were manually restrained. Blood samples were taken from the animals *via* retro orbital puncture for semi-serial bleeding or cardiac puncture (under anesthesia with isoflurane) for terminal bleeding into K2EDTA tubes. Blood samples were put on ice and centrifuged to obtain plasma samples (2,000 *g*, 5 min under 4 °C) within 15 min. The animal was euthanized with pure CO_2 inhalation. A mid-line incision was made on the neck. The muscle under the skin was cut to expose the cisterna magna. The cisterna magna was penetrated with the sharp end of one capillary. The cerebrospinal fluid (CSF) would be sucked spontaneously into the capillary. After CSF collection, a mid-line incision was made in the animal's scalp and skin retracted. The skull overlying the brain was removed. The whole brain was collected, rinsed with cold saline, dried on filtrate paper, weighed, and snap frozen by placing into dry ice. The supernatant diluted with H_2O and methanol (CH_3OH) of each sample (*i.e.*, plasma, brain, and CSF) was injected for LC-MS/MS analysis (Shanghai ChemPartner).

1.4.6. Animal and Drug Administration (APP/PS1 Mice)

Transgenic mice overexpressing the human APP695 [K670N/M671L (Swedish)] and PS1 (M146V) mutations were originated from GlaxoSmithKline (Harlow, UK)[35] and maintained as previously described[50]. Because APP/PS1 mice show sex differences in disease progression, we used only male mice. Data analysis was done in 9.5 months of age. Age and sex matched C57BL/6 mice were used as WT mice. Block randomization method was used to allocate the animals to experimental groups. To eliminate the bias, we were blinded in experimental progress, such as data collection and data analysis. Mice were housed at a 12 h day/12 h night cycle with free access to tap water and food pellets. All protocols were approved by the Kyungpook National University Institutional Animal Care and Use Committee (IACUC). **1** was freshly prepared shortly before treatment by dissolving it in vehicle [85% DMSO in saline], and injected intraperitoneally every morning for 2 months, at the dose of 2 mg/kg of body weight starting at 7.5 months of age.

1.4.7. Behavioral Studies (APP/PS1 Mice)

We performed behavioral studies to assess spatial learning and memory in the Morris water maze (MWM) as previously described[16,50,51]. Animals were given four trials per a day for 10 days to learn the task. At day 11, animals were given a probe trial in which the platform was removed. Fear conditioning was conducted following previously described techniques[50]. On the conditioning day, mice were

ULSAN NATIONAL INSTITUTE OF SCIENCE AND TECHNOLOGY

individually placed into the conditioning chamber. After a 60 s exploratory period, a tone (10 kHz, 70 dB) was delivered for 10 s; this served as the conditioned stimulus (CS). The CS co-terminated with the unconditioned stimulus (US), a scrambled electrical footshock (0.3 mA, 1 s). The CS−US pairing was delivered twice at a 20 s intertrial interval. On day 2, each mouse was placed in the fear-conditioning chamber containing the same exact context, but with no administration of a CS or foot shock. Freezing was analyzed for 5 min. On day 3, a mouse was placed in a test chamber that was different from the conditioning chamber. After a 60 s exploratory period, the tone was presented for 60 s without the footshock. The rate of the freezing response of mice was used to measure the fear memory. The open field test was used for locomotion and anxious behaviors as previously described[16]. The open field box consisted of a square box. Each animal was placed in the box for 10 min. Overall activity in the box was measured, and the amount of time and distance traveled in the center arena was noted. After each trial, the test chambers were cleaned with a damp towel and ddH_2O followed by ethanol (EtOH, 70% v/v). The light and dark test was used for assessing the anxiety-like behavior as previously described[16]. One chamber was brightly illuminated, whereas the other chamber was dark. Mice were placed into the dark chamber and allowed to move freely between the two chambers with the door open for 10 min. The total number of transitions, latency to first enter the light chamber, distance traveled, and time spent in each chamber were recorded.

1.4.8. Histological Analysis (APP/PS1 Mice)

Mice anesthetized were transcardially perfused with PBS to wash out the residual blood from cerebral circulation. After perfusion with PBS, mice were further perfused with 4% paraformaldehyde (PFA) in PBS. Brains were post-fixed in 4% PFA overnight at 4 °C. Brain tissue was then coronal sectioned at a thickness of 30 μm using a vibratome. Thioflavin-S (ThS) staining was carried out according to previously described procedures[51]. We used Iba1 (rabbit, 1:500, 019-19941; Wako Pure Chemical Industries, Ltd., Osaka, Japan), GFAP (rabbit, 1:500, N1506; Dako, CA, USA), and Lamp1 (mouse, 1:200, ab24170; Abcam, Cambridge, UK). The sections were analyzed with a laser-scanning confocal microscope (FV1000; Olympus, Tokyo, Japan) or with a BX51 microscope (Olympus). MetaMorph software (Molecular Devices) was used for quantification. Three-dimensional reconstruction of microglia was recorded and analyzed using IMARIS software (Bitplane, Belfast, UK)[52].

1.4.9. Animal and Drug Administration (5XFAD Mice)

For evaluation of **1**'s *in vivo* efficacy in the AD affected brain, we treated 5XFAD mice, a transgenic animal model of AD overexpressing mutant human APP695 [K670N/M671L (Swedish), I716 V (Florida), and V717I (London)] and PS1 (M146L and L286V)[38], with **1** as previously described[39,40]. Mice were housed at a 12 h day/12 h night cycle with free access to tap water and food pellets. Animal studies with 5XFAD mice were conducted in accordance with the guidelines of the Asan Institute for

ULSAN NATIONAL INSTITUTE OF SCIENCE AND TECHNOLOGY

Life Science for Laboratory Animal Care and Use (Asan Medical Center, Seoul, Republic of Korea). **1** was freshly prepared shortly before treatment by dissolving it in vehicle [1% DMSO v/v; 20 mM HEPES, pH 7.4, 150 mM NaCl], and injected intraperitoneally every morning for consecutive 31 days, at the dose of 1 mg/kg of body weight starting at 3 months of age.

1.4.10. Behavioral Studies (5XFAD Mice)

From the 27th day of the treatment, the performance of spatial learning and memory of the animals was assessed in the MWM with three test trials per a day for 5 days[39,40]. The mice also experienced the probe trials for 60 s in the MWM without the target platform at 3 h after the last MWM test. The test parameters were collected and analyzed on the SMART Video Tracking System (Harvard Apparatus, Holliston, MA, USA).

1.4.11. Histological Analysis (5XFAD Mice)

The deposition of amyloid plaques was assessed on the sagittal sections (12 μm thickness) of the left hemispheres after the immunohistochemistry and histological staining using the human Aβ(17-24)-specific antibody 4G8 (Covance, Princeton, NJ, USA) and Accustain® Congo Red amyloid staining solution (Sigma-Aldrich), respectively. The stained sections were examined or photographed under a light microscope (Eclipse 80i; Nikon, Tokyo, Japan). Amyloid deposits were presented as the percent area of 4G8-immunoreactive deposits or the number of congophilic plaques per mm^2 of the brain regions.

1.4.12. Enzyme-Linked Immunosorbent Assay (ELISA) for Quantification of the Cerebral Aβ (5XFAD Mice)

Amyloid pathology was evaluated as previously described[39,40]. $A\beta_{40}$, $A\beta_{42}$ (Invitrogen, Carlsbad, CA, USA), and oligomeric Aβ (Biosensis, Thebarton, Australia) were measured in PBS-, SDS-, or formic acid (FA)-soluble fractions following the serial centrifugal fractionations of the right cerebral hemispheres by sandwich ELISA.

1.4.13. Primary Cell Culture

Neurons from E18 C57BL/6 mice were prepared as previously described with minor modifications[53]. Cortices were dissected and then dissociated followed by incubation in papain for 15 min at 37 °C. Neurons were plated on poly-L-lysine-coated coverslips with neuronal culture medium, serum-free Neurobasal medium (GIBCO) containing 2% B27 supplements (GIBCO), 1 mM Glutamax supplement (GIBCO), and 100 U/mL penicillin and 100 mg/mL streptomycin (GIBCO) at 37 °C in a humidified atmosphere of 5% CO_2. Primary astrocyte cultures were prepared from C57BL/6 mice as previously described[54]. In brief, after removal of the meninges, postnatal day 7 (P7) mouse brain tissues were

ULSAN NATIONAL INSTITUTE OF SCIENCE AND TECHNOLOGY

minced and incubated in a rocking water bath at 37 °C for 30 min in the presence of 0.25% trypsin-EDTA (Sigma-Aldrich). Enzyme-digested dissociated cells were triturated with astrocyte-specific medium (DMEM/F12 containing 10% FBS, 0.2 and 1% penicillin-streptomycin) and centrifuged at 1,300 rpm for 8 min. The pellet was resuspended in DMEM/F12, passed through a 40-μm cell strainer. The filtrate was allowed for pre-adherence for 30 min to remove any contamination from fibroblasts before being seeded in dishes and added the astrocyte-specific medium. For astrocytes splitting, dishes were added with Ara-C and placed in a heated shaker for 6-7 h. The medium was removed from the dishes, and trypsin-EDTA was added to the dish and incubated for 5-10 min at 37 °C. After centrifugation at 1,300 rpm for 8 min, the supernatant was removed and the astrocytes were maintained in culture by feeding every 1-2 weeks with astrocyte-specific medium. Primary microglia were isolated from the mice brain as previously described[55]. The cortex of WT (1-month-old) mice were minced in the Hibernate A (GIBCO)/B27 (Invitrogen) medium and dissociated using papain (Worthington Biochemical Corporation, NJ, USA) solution. After tissue trituration, cells were separated by Optiprep (Sigma-Aldrich) density gradient centrifugation. Fractionated microglia were cultured in DMEM/F12 containing 10% FBS, 0.2 and 1% penicillin-streptomycin. We confirmed the successful isolation of primary cells from the brains of mice following each published methods[53,54,55].

1.4.14. Aβ-Mediated Inflammatory Response in Various Cells

$A\beta_{42}$ (Invitrogen) was solubilized in 10% DMSO, to a stock concentration of 500 μM. The $A\beta_{42}$ solution was then incubated at 37 °C for 7 days to produce aggregated forms (*i.e.*, containing oligomeric and fibrillar Aβ). To examine inflammatory responses *in vitro*, $A\beta_{42}$ (10 μM) was treated in microglia or astrocytes with and without **1** (10 μM). After 24 h, the CM derived from microglia or astrocytes was discarded, and the fresh medium was added into each cell. One day later, microglia or astrocytes were collected for analysis of inflammatory cytokines and the CM derived from microglia or astrocytes was transferred to the astrocytes (CM derived from microglia) or microglia (CM derived from astrocytes). After 24 h, astrocytes or microglia were collected for analysis of inflammatory cytokines. To investigate the effects of Off/On signals derived from neuron to microglia, neurons were treated with $A\beta_{42}$ (10 μM) or $A\beta_{42}$ (10 μM) with **1** (10 μM). After 24 h, the CM derived from neurons was discarded, and fresh medium was added into the neurons. One day later, neurons were collected to analyze for Off/On signals and the CM derived from neurons was transferred to the microglia. After 24 h, microglia were collected for analysis of inflammatory cytokines.

1.4.15. Western Blotting for NLRP3-Related Protein Experiments

Brain samples were lysed in RIPA buffer (Cell Signaling Technology, MA, USA), then subjected to sodium dodecyl sulfate-polyacrylamide gel electrophoresis (SDS-PAGE) and transferred to a

ULSAN NATIONAL INSTITUTE OF SCIENCE AND TECHNOLOGY

nitrocellulose membrane. Membranes were blocked with 5% milk, incubated with a primary antibody and then incubated with an appropriate horseradish peroxidase-conjugated secondary antibody[50]. Primary antibodies to the following proteins were used: NLRP3 (rabbit, 1:1,000; 15101, Cell Signaling Technology), ASC (rabbit, 1:1,000; 67824, Cell Signaling Technology), Caspase 1 (mouse, 1:1,000; AG-20B-0042, Adipogen Life Sciences, CA, USA), IL-1β (mouse, 1:1000; 12242, Cell Signaling Technology), and β-actin (1:1,000; SC-47778, Santa Cruz Biotechnology, TX, USA). Rabbit-HRP (1:1,000; 7074s, Cell Signaling Technology) and mouse-HRP (1:1,000; sc2005, Santa Cruz Biotechnology) were used as the secondary antibody. We performed densitometric quantification using the ImageJ software (National Institutes of Health, ME, USA). Images have been cropped for presentation.

1.4.16. Aβ Aggregation Experiments

All experiments were preformed according to previously published methods[39,40,56]. Prior to experiments, Aβ peptides were dissolved in ammonium hydroxide (NH_4OH, 1% v/v aq), aliquoted, lyophilized overnight, and stored at -80 °C. A stock solution of Aβ was prepared by dissolving lyophilized peptide in 1% NH_4OH (10 μL) and followed by dilution in ddH_2O. The concentration of Aβ was determined by measuring the absorbance of the solution at 280 nm (ε = 1450 $M^{-1}cm^{-1}$ for $A\beta_{40}$; ε = 1490 $M^{-1}cm^{-1}$ for $A\beta_{42}$). The buffered solution (20 mM HEPES, pH 7.4, 150 mM NaCl) was used for preparation of Aβ samples. For the inhibition studies, **1** (50 μM) was added to a solution containing Aβ (25 μM) and incubated for 24 h at 37 °C with constant agitation (250 rpm). For the disaggregation studies, Aβ was incubated for 24 h at 37 °C with constant agitation prior to treatment with **1** (50 μM). The resulting samples containing Aβ (pre-incubated for 24 h) and **1** were incubated for an additional 24 h at 37 °C with constant agitation.

1.4.17. Gel Electrophoresis and Western Blotting

The Aβ samples from the inhibition and disaggregation experiments were analyzed by gel/Western blot utilizing an anti-Aβ antibody (6E10) following previously reported procedures[39,40,56]. Samples (10 μL) were separated on a 10-20% Tris-tricine gel (Invitrogen). Following separation, the proteins were transferred onto nitrocellulose membranes, which was blocked with bovine serum albumin (BSA, 3% w/v, RMBIO, Missoula, MT, USA) in Tris-buffered saline (TBS) containing 0.1% Tween-20 (TBS-T) for 4 h at room temperature or overnight at 4 °C. The membranes were incubated with 6E10 (1:2000, Covance) in a solution of 2% BSA (w/v in TBS-T) for 4 h at room temperature or overnight at 4 °C. After washing with TBS-T three times (10 min each), the horseradish peroxidase-conjugated goat anti-mouse secondary antibody (1:5000, Cayman Chemical Company, Ann Arbor, MI, USA) in 2% BSA

ULSAN NATIONAL INSTITUTE OF SCIENCE AND TECHNOLOGY

was added for 2 h at room temperature. A homemade ECL kit[39,40,56] was then used to visualize the results on a ChemiDoc MP Imaging System (Bio-Rad).

1.4.18. Transmission Electron Microscopy

$A\beta_{40}$ samples for TEM measurements were prepared following previously reported methods[39,40,56]. Glow discharged grids (Formvar/Carbon 300-mesh, Electron Microscopy Sciences, Hatfield, PA, USA) were treated with the samples (5 μL) of (i) compound-free $A\beta_{40}$ aggregates and (ii) $A\beta_{40}$ aggregates incubated with **1** for 2 min at room temperature. Excess sample was removed with filter paper and the grids were washed with ddH_2O three times. Each grid was stained with uranyl acetate (1% w/v ddH_2O; 5 μL) for 1 min. Uranyl acetate was blotted off and grids were dried for at least 20 min at room temperature. Images of samples were obtained by a JEOL JEM-2100 transmission electron microscope (200 kV; 25,000x magnification; UCRF). For the TEM studies, we randomly picked the locations of samples on the grids for taking images and collected more than 20 images from each grid.

1.4.19. RNA Isolation and Real-Time PCR Analysis

RNA was extracted from brain homogenates and cell lysates using the RNeasy Lipid Tissue Mini kit and RNeasy Plus Mini kit (QIAGEN, Hilden, Germany) according to the manufacturer's instructions. cDNA was synthesized from 5 μg of total RNA using a commercially available kit (Takara Bio Inc., Shiga, Japan). Quantitative real-time PCR was performed using a Corbett research RG-6000 real-time PCR instrument. The used primers in this study are described in Supplementary Table 1.

1.4.20. Statistics

Sample sizes were determined by G-Power software (with $\alpha = 0.05$ and power of 0.8). In general, statistical methods were not used to re-calculate or predetermine sample sizes. Variance was similar within comparable experimental groups. Experimenters were blinded to the identity of experimental groups until the end of data collection and analysis for at least one of the independent experiments. Comparisons between two groups were performed with Student's *t*-test. In cases where more than two groups were compared to each other, an One-way analysis of variance (ANOVA) was used, followed by Tukey's HSD test or Student-Newman-Keuls post hoc test. All statistical analyses were performed using SPSS statistical software. All values were denoted as mean s.e.m. Statistical difference was considered significant at $*P < 0.05$, $**P < 0.01$, $***P < 0.001$.

1.5. Acknowledgments

This research is supported by the National Research Foundation of Korea (NRF) grant funded by the Korean government [NRF-2016R1A5A1009405 and NRF-2017R1A2B3002585 (to M.H.L); NRF-2015R1A2A1A15052049 (to J.-Y.L.); NRF-2017R1A4A1015652 and NRF-2018M3C7A1056513 (to

ULSAN NATIONAL INSTITUTE OF SCIENCE AND TECHNOLOGY

H.K.J.)]; the Korea Advanced Institute of Science and Technology (KAIST) (M.H.L.). J.K. thanks the Global Ph.D. fellowship program for support through the National Research Foundation of Korea (NRF) funded by the Ministry of Education (NRF-2015HIA2A1030823). This research was also supported by a grant of the Korea Health Technology R&D Project through the KHIDI, funded by the Ministry of Health & Welfare, Republic of Korea (HI16C2131,) (to J.S.B.).

1.6. References

1. Przedborski, S.; Vila, M.; Jackson-Lewis, V., *J. Clin. Invest.* **2003,** *111*, 3-10.
2. Heneka, M. T.; Carson, M. J.; El Khoury, J.; Landreth, G. E.; Brosseron, F.; Feinstein, D. L.; Jacobs, A. H.; Wyss-Coray, T.; Vitorica, J.; Ransohoff, R. M.; Herrup, K.; Frautschy, S. A.; Finsen, B.; Brown, G. C.; Verkhratsky, A.; Yamanaka, K.; Koistinaho, J.; Latz, E.; Halle, A.; Petzold, G. C.; Town, T.; Morgan, D.; Shinohara, M. L.; Perry, V. H.; Holmes, C.; Bazan, N. G.; Brooks, D. J.; Hunot, S.; Joseph, B.; Deigendesch, N.; Garaschuk, O.; Boddeke, E.; Dinarello, C. A.; Breitner, J. C.; Cole, G. M.; Golenbock, D. T.; Kummer, M. P., *Lancet Neurol.* **2015,** *14*, 388-405.
3. Hirsch, E. C.; Hunot, S., *Lancet Neurol.* **2009**, *8*, 382-397.
4. Philips, T.; Robberecht, W., *Lancet Neurol.* **2011**, *10*, 253-263.
5. Ransohoff, R. M., *Science* **2016**, *353*, 777-783.
6. Kreutzberg, G. W., *Trends Neurosci.* **1996**, *19*, 312-318.
7. Heppner, F. L.; Ransohoff, R. M.; Becher, B., *Nat. Rev. Neurosci.* **2015**, *16*, 358-372.
8. Hanisch, U. K.; Kettenmann, H., *Nat. Neurosci.* **2007**, *10*, 1387-1394.
9. Hickman, S. E.; Allison, E. K.; El Khoury, J., *J. Neurosci.* **2008**, *28*, 8354-8360.
10. Block, M. L.; Zecca, L.; Hong, J. S., *Nat. Rev. Neurosci.* **2007**, *8*, 57-69.
11. Tuppo, E. E.; Arias, H. R., *Int. J. Biochem. Cell Biol.* **2005**, *37*, 289-305.
12. Tansey, M. G.; Goldberg, M. S., *Neurobiol. Dis.* **2010**, *37*, 510-518.
13. Prince, M.; Comas-Herrera, A.; Knapp, M.; Guerchet, M.; Karagiannidou, M., **2016**.
14. Savelieff, M. G.; Nam, G.; Kang, J.; Lee, H. J.; Lee, M.; Lim, M. H., *Chem. Rev.* **2018**. (DOI: 10.1021/acs.chemrev.8b00138)
15. Haass, C.; Selkoe, D. J., *Nat. Rev. Mol. Cell Biol.* **2007**, *8*, 101-112.
16. Lee, J. Y.; Han, S. H.; Park, M. H.; Baek, B.; Song, I. S.; Choi, M. K.; Takuwa, Y.; Ryu, H.; Kim, S. H.; He, X.; Schuchman, E. H.; Bae, J. S.; Jin, H. K., *Nat. Commun.* **2018**, *9*, 1479.
17. Perry, V. H.; Holmes, C., *Nat. Rev. Neurol.* **2014**, *10*, 217-224.
18. Bachstetter, A. D.; Norris, C. M.; Sompol, P.; Wilcock, D. M.; Goulding, D.; Neltner, J. H.; St Clair, D.; Watterson, D. M.; Van Eldik, L. J., *J. Neurosci.* **2012**, *32*, 10201-10210.
19. Mandrekar-Colucci, S.; Karlo, J. C.; Landreth, G. E., *J. Neurosci.* **2012**, *32*, 10117-10128.
20. Medeiros, R.; Kitazawa, M.; Passos, G. F.; Baglietto-Vargas, D.; Cheng, D.; Cribbs, D. H.; LaFerla, F. M., *Am. J. Pathol.* **2013**, *182*, 1780-1789.

ULSAN NATIONAL INSTITUTE OF SCIENCE AND TECHNOLOGY

21. Ano, Y.; Dohata, A.; Taniguchi, Y.; Hoshi, A.; Uchida, K.; Takashima, A.; Nakayama, H., *J. Biol. Chem.* **2017**, *292*, 3720-3728.
22. Coll, R. C.; Robertson, A. A.; Chae, J. J.; Higgins, S. C.; Munoz-Planillo, R.; Inserra, M. C.; Vetter, I.; Dungan, L. S.; Monks, B. G.; Stutz, A.; Croker, D. E.; Butler, M. S.; Haneklaus, M.; Sutton, C. E.; Nunez, G.; Latz, E.; Kastner, D. L.; Mills, K. H.; Masters, S. L.; Schroder, K.; Cooper, M. A.; O'Neill, L. A., *Nat. Med.* **2015**, *21*, 248-255.
23. Dempsey, C.; Rubio Araiz, A.; Bryson, K. J.; Finucane, O.; Larkin, C.; Mills, E. L.; Robertson, A. A. B.; Cooper, M. A.; O'Neill, L. A. J.; Lynch, M. A., *Brain Behav. Immun.* **2017**, *61*, 306-316.
24. Ouellet, M.; Percival, M. D., *Arch Biochem. Biophys.* **2001**, *387*, 273-280.
25. Amar, P. J.; Schiff, E. R., *Expert. Opin. Drug. Saf.* **2007**, *6*, 341-355.
26. Ryu, Y. S.; Lee, J. H.; Seok, J. H.; Hong, J. H.; Lee, Y. S.; Lim, J. H.; Kim, Y. M.; Hur, G. M., *Biochem. Biophys. Res. Commun.* **2000**, *272*, 758-764.
27. Mancini, F.; Landolfi, C.; Muzio, M.; Aquilini, L.; Soldo, L.; Coletta, I.; Guglielmotti, A.; Mantovani, A.; Pinza, M.; Milanese, C., *Neurosci. Lett.* **2003**, *353*, 79-82.
28. Maharaj, D. S.; Saravanan, K. S.; Maharaj, H.; Mohanakumar, K. P.; Daya, S., *Neurochem. Int.* **2004**, *44*, 355-360.
29. Locke, C. J.; Fox, S. A.; Caldwell, G. A.; Caldwell, K. A., *Neurosci. Lett.* **2008**, *439*, 129-133.
30. Tripathy, D.; Grammas, P., *J. Neuroinflammation* **2009**, *6*, 10.
31. Pitchaimani, V.; Arumugam, S.; Thandavarayan, R. A.; Thiyagarajan, M. K.; Aiyalu, R.; Sreedhar, R.; Nakamura, T.; Watanabe, K., *J. Clin. Biochem. Nutr.* **2012**, *50*, 241-244.
32. Bisaglia, M.; Venezia, V.; Piccioli, P.; Stanzione, S.; Porcile, C.; Russo, C.; Mancini, F.; Milanese, C.; Schettini, G., *Neurochem. Int.* **2002**, *41*, 43-54.
33. Zhao, W. X.; Zhang, J. H.; Cao, J. B.; Wang, W.; Wang, D. X.; Zhang, X. Y.; Yu, J.; Zhang, Y. Y.; Zhang, Y. Z.; Mi, W. D., *J. Neuroinflammation* **2017**, *14*, 17.
34. Laine, J. E.; Auriola, S.; Pasanen, M.; Juvonen, R. O., *Xenobiotica* **2009**, *39*, 11-21.
35. Howlett, D. R.; Richardson, J. C.; Austin, A.; Parsons, A. A.; Bate, S. T.; Davies, D. C.; Gonzalez, M. I., *Brain Res.* **2004**, *1017*, 130-136.
36. Mucke, L.; Selkoe, D. J., *Cold Spring Harb. Perspect. Med.* **2012**, *2*, a006338.
37. Urbanc, B.; Cruz, L.; Le, R.; Sanders, J.; Ashe, K. H.; Duff, K.; Stanley, H. E.; Irizarry, M. C.; Hyman, B. T., *Proc. Natl. Acad. Sci. U. S. A.* **2002**, *99*, 13990-13995.
38. Oakley, H.; Cole, S. L.; Logan, S.; Maus, E.; Shao, P.; Craft, J.; Guillozet-Bongaarts, A.; Ohno, M.; Disterhoft, J.; Van Eldik, L.; Berry, R.; Vassar, R., *J. Neurosci.* **2006**, *26*, 10129-10140.
39. Derrick, J. S.; Kerr, R. A.; Nam, Y.; Oh, S. B.; Lee, H. J.; Earnest, K. G.; Suh, N.; Peck, K. L.; Ozbil, M.; Korshavn, K. J.; Ramamoorthy, A.; Prabhakar, R.; Merino, E. J.; Shearer, J.; Lee, J. Y.; Ruotolo, B. T.; Lim, M. H., *J. Am. Chem. Soc.* **2015**, *137*, 14785-14797.
40. Beck, M. W.; Derrick, J. S.; Kerr, R. A.; Oh, S. B.; Cho, W. J.; Lee, S. J.; Ji, Y.; Han, J.; Tehrani,

ULSAN NATIONAL INSTITUTE OF SCIENCE AND TECHNOLOGY

Z. A.; Suh, N.; Kim, S.; Larsen, S. D.; Kim, K. S.; Lee, J. Y.; Ruotolo, B. T.; Lim, M. H., *Nat. Commun.* **2016**, *7*, 13115.

41. Lee, S. J.; Nam, E.; Lee, H. J.; Savelieff, M. G.; Lim, M. H., *Chem. Soc. Rev.* **2017**, *46*, 310-323.
42. Dowling, P.; Clynes, M., *Proteomics* **2011**, *11*, 794-804.
43. Biber, K.; Neumann, H.; Inoue, K.; Boddeke, H. W., *Trends Neurosci.* **2007**, *30*, 596-602.
44. Guillot-Sestier, M. V.; Doty, K. R.; Gate, D.; Rodriguez, J., Jr.; Leung, B. P.; Rezai-Zadeh, K.; Town, T., *Neuron* **2015**, *85*, 534-548.
45. Karperien, A.; Ahammer, H.; Jelinek, H. F., *Front. Cell. Neurosci.* **2013**, *7*, 3.
46. Krabbe, G.; Halle, A.; Matyash, V.; Rinnenthal, J. L.; Eom, G. D.; Bernhardt, U.; Miller, K. R.; Prokop, S.; Kettenmann, H.; Heppner, F. L., *PLoS One* **2013**, *8*, e60921.
47. Heneka, M. T.; Kummer, M. P.; Stutz, A.; Delekate, A.; Schwartz, S.; Vieira-Saecker, A.; Griep, A.; Axt, D.; Remus, A.; Tzeng, T. C.; Gelpi, E.; Halle, A.; Korte, M.; Latz, E.; Golenbock, D. T., *Nature* **2013**, *493*, 674-678.
48. Liu, Y.; Yao, W.; Xu, J.; Qiu, Y.; Cao, F.; Li, S.; Yang, S.; Yang, H.; Wu, Z.; Hou, Y., *Innate. Immun.* **2015**, *21*, 587-597.
49. Hamley, I. W., *Chem. Rev.* **2012**, *112*, 5147-5192.
50. Lee, J. K.; Jin, H. K.; Park, M. H.; Kim, B. R.; Lee, P. H.; Nakauchi, H.; Carter, J. E.; He, X.; Schuchman, E. H.; Bae, J. S., *J. Exp. Med.* **2014**, *211*, 1551-1570.
51. Lee, J. K.; Schuchman, E. H.; Jin, H. K.; Bae, J. S., *Stem Cells* **2012**, *30*, 1544-1555.
52. Goldmann, T.; Wieghofer, P.; Muller, P. F.; Wolf, Y.; Varol, D.; Yona, S.; Brendecke, S. M.; Kierdorf, K.; Staszewski, O.; Datta, M.; Luedde, T.; Heikenwalder, M.; Jung, S.; Prinz, M., *Nat. Neurosci.* **2013**, *16*, 1618-1626.
53. Lee, J. K.; Jin, H. K.; Bae, J. S., *Curr. Alzheimer Res.* **2010**, *7*, 540-548.
54. Albuquerque, C.; Joseph, D. J.; Choudhury, P.; MacDermott, A. B., *Cold Spring Harb. Protoc.* **2009**, *2009*, pdb prot5273.
55. Brewer, G. J.; Torricelli, J. R., *Nat. Protoc.* **2007**, *2*, 1490-1498.
56. Lee, S.; Zheng, X.; Krishnamoorthy, J.; Savelieff, M. G.; Park, H. M.; Brender, J. R.; Kim, J. H.; Derrick, J. S.; Kochi, A.; Lee, H. J.; Kim, C.; Ramamoorthy, A.; Bowers, M. T.; Lim, M. H., *J. Am. Chem. Soc.* **2014**, *136*, 299-310.

ULSAN NATIONAL INSTITUTE OF SCIENCE AND TECHNOLOGY

Chapter 2.

A Near-Infrared Fluorescent Probe for Amyloid-β Aggregates

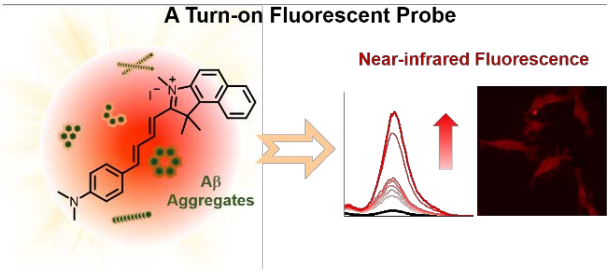

The results that described in this Chapter was recently published in *Dyes Pigments* as a research article. I conducted all fluorescence experiments and characterization of Aβ aggregates, as well as wrote the paper, in collaboration with Mingeun Kim and Dr. Hyuck Jin Lee. The synthesis of the compound and the calculation of its quantum yield were carried out by Anjong Florence Tikumc, Vijayan Thamilarasanc, and Professor Jinheung Kim. I appreciate Professor Lim for her guidance and care throughout all the experiments and writing of this research article.

Misun Lee[§], Mingeun Kim[§], Anjong Florence Tikum[§], Hyuck Jin Lee, Vijayan Thamilarasan, Mi Hee Lim, Jinheung Kim, A Near-Infrared Fluorescent Probe for Amyloid-β Aggregates, *Dyes Pigm.*, **2019**, *162*, 97-103. ([§]Co-first authorship)

ULSAN NATIONAL INSTITUTE OF SCIENCE AND TECHNOLOGY

2.1. Introduction

Alzheimer's disease (AD), a chronic neurodegenerative disease, is characterized by the accumulation of amyloid-β (Aβ) deposits in the brain[1-3]. Aβ deposits are mainly composed of the aggregates of two isoforms, $A\beta_{40}$ and $A\beta_{42}$[2,3]. Upon peptide aggregation, various Aβ aggregates, including oligomers, protofibrils, and fibrils, are generated showing their distinct biological properties (*e.g.*, toxicity)[4-6]. Among Aβ aggregates, several studies indicate that oligomers and fibrils are involved in toxicity[5,7-10]. Thus, effective tactics to identify Aβ aggregates have been recently developed. Along with thioflavin-T (ThT), a widely used probe for sensing β-sheet-rich Aβ aggregates[11], emissive probes for optical sensing and imaging of Aβ deposits have been devised to evaluate and monitor the progression of AD[12-32]. Effective emissive probes for Aβ deposits should possess emission wavelength in the near-infrared (near-IR) region for having less photo-induced damage of cellular components and for minimizing the background fluorescence from the brain tissue[16-27].

Chemical probes containing donor-π-acceptor and donor-π-acceptor-π-donor systems, such as **AOI987**, **CRANAD-2**, **NIAD-4**, and **SN2**, were developed for the detection of Aβ plaques with near-IR fluorescent signals[15,16,18,19,27,31,32]. To construct the electron push-pull models, the design utilized the structures of 4-methylmorpholine, dimethylaminostyrene, and phenol as the donors as well as the difluoroboronate, pyrone, and dicyano groups as the acceptors[15,16,18,19,27,31,32]. Fluorescent probes containing a donor-π-acceptor system, composed of a dimethylaminostyrene group and a conjugated linker between the donor and acceptor, were reported to have a nanomolar range of the binding affinity (K_d) for Aβ fibrils[15,19,27]. Although they showed some changes in fluorescence upon binding to Aβ fibrils, the emission maximum of the probes ranged from 504 nm to 661 nm[15,19,27].

Herein, we report a turn-on near-IR fluorescent probe (**2**; Scheme 2.1) capable of detecting Aβ aggregates upon the progression of Aβ aggregation at *ca.* 710 nm. Our probe, **2**, is composed of a π-conjugated bridge between dimethylaminostyrene and benzo[*e*]indole groups. Although a sensor having a similar structure was previously reported for another purpose (*i.e.*, detection of SO_3^{2-} and SO_4^{2-}/HSO_4^-)[33], **2** was evaluated in the present study as a probe capable of detecting Aβ aggregates based on fluorescence at the distinctly separated near-IR region. Our non-emissive probe, **2**, exhibits turn-on fluorescence upon incubation with Aβ aggregates. In addition, the fluorescence intensity of **2** was varied based on the aggregation states of Aβ, suggesting the utility of the probe in monitoring Aβ aggregation. Furthermore, **2** presents turn-on fluorescence with Aβ aggregates in living cells, along with no toxicity under the condition used for live-cell imaging.

ULSAN NATIONAL INSTITUTE OF SCIENCE AND TECHNOLOGY

Scheme 2.1. Synthetic route to **2**.

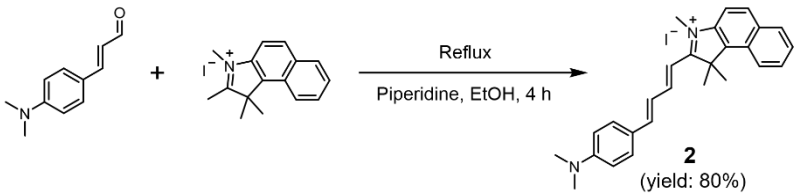

2.2. Results and Discussion

2.2.1. Design and Synthesis of Probe 2

The styrene-based fluorescence probe, **2**, was designed for imaging Aβ aggregates and prepared as shown in Scheme **2**. The structure of **2** contains (i) the dimethylamino functionality as an Aβ-interacting moiety[17] and an electron donor and (ii) the benzo[*e*]indole group as an electron acceptor. Such an electron donor-acceptor unit in the conjugation system leads to decreasing the non-radiative decay rate and consequently increasing the emission intensity due to the hindrance of the internal molecular rotation of the probe[42]. In addition, to gain fluorescent signals at the near-IR region, the length of the π-conjugation was adjusted. The synthesized compound, **2**, was confirmed by NMR spectroscopy and mass spectrometry (Figure 2.1).

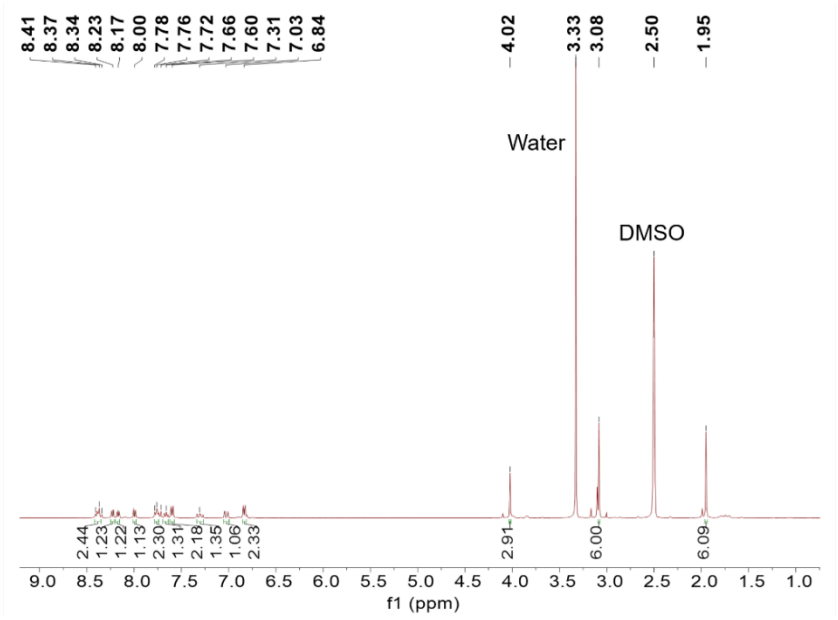

Figure 2.1. ^{1}H NMR spectrum of **2** in DMSO-d_6.

2.2.2. Fluorescent Responses of 2 to Aβ Aggregates

In an organic solvent (*i.e.*, CH_3CN), the absorption and emission bands of **2** were observed at 568 nm and 690 nm, respectively (Figure 2.2). The probe displayed the absorption bands at 479 and 589 nm and the emission peak at *ca.* 700 nm in a buffered solution (pH 7.4) (Figure 2.2 and 2.3). As expected

ULSAN NATIONAL INSTITUTE OF SCIENCE AND TECHNOLOGY

from the longer conjugation linker of the probe (Scheme 2.1), the absorption and emission wavelengths of **2** were higher than those of the styrylpyran derivatives[15,19,27].

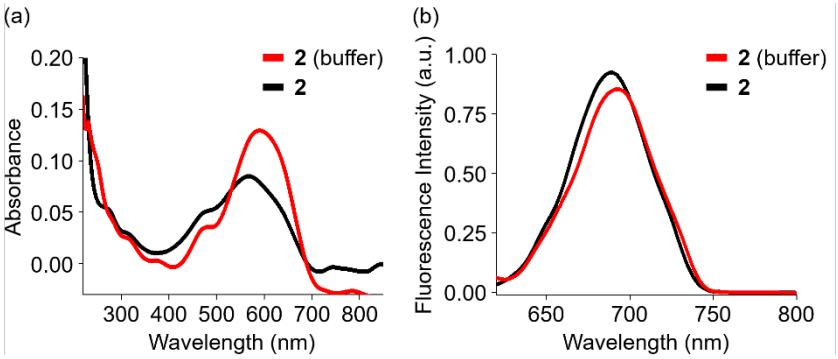

Figure 2.2. Absorption (a) and emission (b) spectra of **2** in the buffered solution (red) and CH_3CN (black). Conditions: [**2**] = 2 μM; 10 mM PBS buffer, pH 7.4; λ_{ex} = 600 nm.

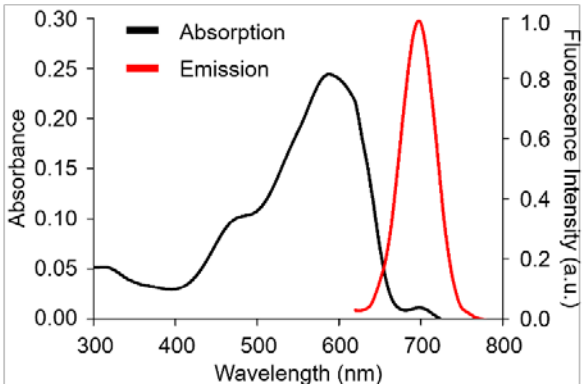

Figure 2.3. Absorption and emission spectra of **2**. Conditions: [**2**] = 3 μM; 10 mM PBS buffer, pH 7.4; λ_{ex} = 600 nm.

Since Aβ peptides have different aggregation states and multiple polymorphs (*e.g.*, monomers, oligomers, and fibrils) during their aggregation pathways following the phases of lag, elongation, and plateau[4,7,43,44], the ability of fluorescent probes to detect Aβ could be varied depending on the type of peptide aggregates[14-27,45-49]. To determine the fluorescent response of **2** to a variety of Aβ species, including monomers, oligomers, or fibrils, Aβ species prepared at different incubation time points were treated with the probe (Figure 2.4). In the buffered solution (pH 7.4), the fluorescence intensities of **2** were noticeably elevated at *ca.* 710 nm with excitation at 574 nm in the presence of Aβ aggregates (10 equiv), in contrast to the weak fluorescence in the absence of Aβ (Figure 2.4a and b; black). In detail, the fluorescence intensity of **2** was gradually increased with treatment of $Aβ_{40}$ species generated upon aggregation (up to 5 h pre-incubation; Figure 2.4a, left) and decreased with $Aβ_{40}$ aggregates produced upon longer incubation, 10 and 12 h incubation (Figure 2.4a, right). In the case of $Aβ_{42}$, **2** exhibited the change in fluorescence, similar to $Aβ_{40}$ species (Figure 2.4b). **2** displayed the enhanced fluorescence

ULSAN NATIONAL INSTITUTE OF SCIENCE AND TECHNOLOGY

with aggregated Aβ [in particular, Aβ aggregates produced by 3-5 h incubation rather than those by 12 h incubation (larger aggregates) (vide infra)].

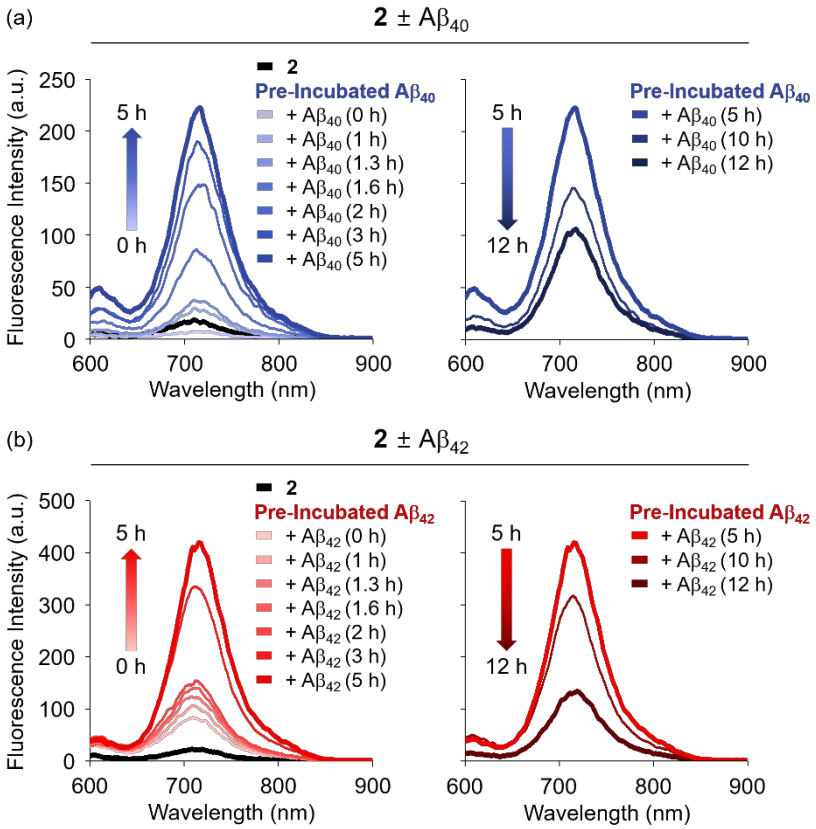

Figure 2.4. Fluorescent responses of **2** to the aggregates of (a) $A\beta_{40}$ and (b) $A\beta_{42}$. Conditions: [Aβ] = 20 μM; [**2**] = 2 μM; 20 mM HEPES, pH 7.4, 150 mM NaCl; 10 min incubation of **2** with Aβ species prior to measurements; λ_{ex} = 574 nm; experiments were conducted in triplicate.

To confirm that the change in fluorescence of **2** resulted from the interaction with Aβ aggregates over other possibilities, such as the self-assembly of the probe through π-stacking, its fluorescence at different concentrations was measured. The fluorescence intensity of **2** was enhanced proportionally as a function of its concentration (0.5-3.0 μM) in the absence of Aβ peptides (Figure 2.5), indicating that the emerged fluorescence of the probe was mainly from the interaction with Aβ aggregates and was not be from its self-aggregating effect. Moreover, to identify that **2** behaves as a molecular rotor, similar to ThT[42,50], the fluorescence intensity of the probe was monitored as a function of the viscosity of the solution. As depicted in Figure 2.6, the fluorescence intensity of **2** was gradually increased as the amount of glycerol in a mixture of MeOH and glycerol was enhanced. This presents that the elevated viscosity of the solution hinders the non-radiative decay of **2**, which suggests the probe as a rotor[50-53].

ULSAN NATIONAL INSTITUTE OF SCIENCE AND TECHNOLOGY

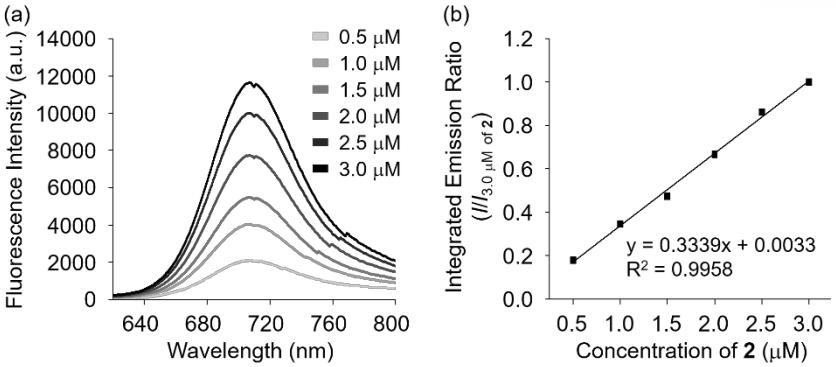

Figure 2.5. Change in the fluorescence intensity of **2** at various concentrations. (a) Fluorescence spectra of **2** and (b) a plot of the integrated fluorescence of **2** as a function of its concentration. Conditions: [**2**] = 0.5, 1, 1.5, 2, 2.5, and 3 μM; 10 mM PBS buffer, pH 7.4; λ_{ex} = 600 nm.

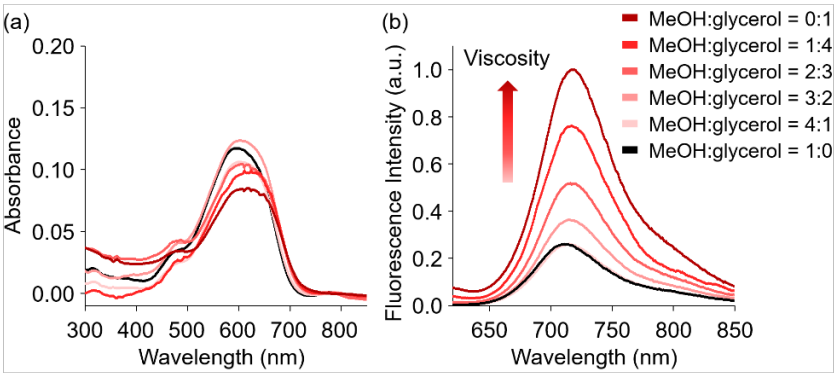

Figure 2.6. Absorption (a) and emission (b) spectra of **2** in a mixture of MeOH and glycerol with different ratios (MeOH:glycerol =1:0, 4:1, 3:2, 2:3, 1:4, and 0:1). Conditions: [**2**] = 2 μM; λ_{ex} = 600 nm.

2.2.3. Identification of Aβ Species Generated at Various Incubation Time Points

To trace the preference of **2** towards the structures of Aβ aggregates generated during peptide aggregation, the kinetic of Aβ aggregation as well as the Aβ species produced following the incubation time were determined (Figure 2.7). The formation of β-sheet-rich aggregates of Aβ was investigated by the ThT assay (Figure 2.7a and d)[11,34]. In addition, the structural information of Aβ aggregates was obtained by the dot blot assay with three distinct antibodies, 6E10 (for Aβ species)[54,55], A11 (for structured oligomeric Aβ)[54], and OC (for fibrillar Aβ)[54], as well as transmission electron microscopy (TEM) (Figure 2.7b, c, e, and f). In the case of $Aβ_{40}$, the short lag phase of Aβ aggregation was observed (from 0 to 0.6 h) followed by the phases of elongation (0.6-2 h) and plateau (after 2 h) (Figure 2.7a). The increased fluorescence intensity of ThT implies that more β-sheet-rich Aβ aggregates are formed with longer incubation of the peptide[11]. Based on the dot blot assay, the gradual generation and maintenance of structured oligomers and fibrils were monitored from 0.6 to 10 h by A11 and OC, respectively (Figure 2.7b). After 10 h, the existence of fibrillar forms of $Aβ_{40}$ was identified by OC;

ULSAN NATIONAL INSTITUTE OF SCIENCE AND TECHNOLOGY

however, less distinguishable dots were identified in $A\beta_{40}$ samples by A11, suggesting that fewer amounts of structured oligomers may be present in the samples (Figure 2.7b). As the results by the ThT and dot blot assays indicated, more fibrils were recorded by TEM with longer incubation of $A\beta_{40}$ (Figure 2.7c). For $A\beta_{42}$, its aggregation kinetic was similar to that of $A\beta_{40}$, except for the shorter lag phase (Figure 2.7d). On the basis of the obtained data from the dot blot assay and TEM, as $A\beta_{42}$ was incubated longer, more fibrils were detected, along with structured oligomers (Figure 2.7e and f). Taken both the results from the fluorescent responses of **2** to Aβ aggregates and the aggregation kinetics of Aβ peptides together, our probe could detect aggregated Aβ species, including structured oligomers and less matured fibrils.

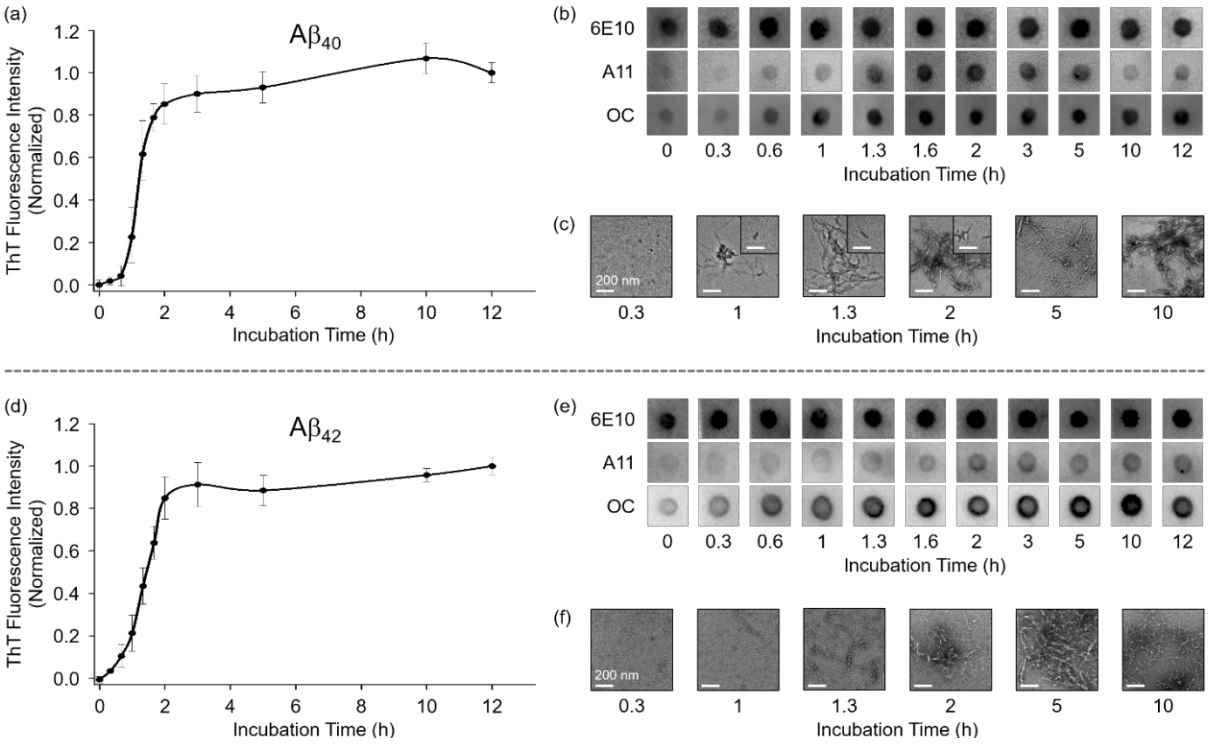

Figure 2.7. Aggregation kinetics and conformations of $A\beta_{40}$ and $A\beta_{42}$. The aggregation of $A\beta_{40}$ (top) and $A\beta_{42}$ (bottom) was identified by (a and d) the ThT assay, (b and e) the dot blot assay, and (c and f) TEM. Conditions: [Aβ] = 20 μM; 20 mM HEPES, pH 7.4, 150 mM NaCl; 37 °C; constant agitation; λ_{ex} = 440 nm, λ_{em} = 490 nm (for the ThT assay). Scale bars = 200 nm.

ULSAN NATIONAL INSTITUTE OF SCIENCE AND TECHNOLOGY

2.2.4. Detection Limit and Specificity of 2 towards Aβ Aggregates

The detection limit and specificity of **2** for Aβ species were determined (Figure 2.8). Below the 0.5 equiv of pre-incubated (5 h) Aβ species to **2** (2 μM), no distinguishable change in fluorescence was indicated (Figure 2.8a). On the other hand, the treatment of **2** with one or higher equiv of Aβ species noticeably indicated an increase in fluorescence, suggesting that at least one equiv of Aβ is required for **2** to monitor Aβ species under our experimental conditions (Figure 2.8a). In addition, the fluorescent response of **2** to ubiquitin, a non-amyloidogenic protein containing all secondary structures[56], was measured to verify the probe's specificity towards the amyloidogenic peptide, Aβ (Figure 2.8b). Compared to the remarkable turn-on fluorescence of **2** for Aβ aggregates, its incubation with ubiquitin did not show the altered fluorescence (Figure 2.8b), indicating that our probe could be a sensor for Aβ aggregates. Moreover, the fluorescence quantum yield of **2** was determined in the presence and absence of $A\beta_{42}$ aggregates with methylene blue as the standard in water (Φ_F = 1.8 and 0.35, respectively).

Furthermore, in order to validate if **2** could modify the structure of pre-formed Aβ aggregates during the measurement of its fluorescence, the morphologies of Aβ aggregates upon the treatment of the probe were observed by TEM. As shown in Figure 2.9, although the interactions between **2** and Aβ species were expected based on the varied fluorescence of the probe, the distinguishable morphological alteration of Aβ aggregates after incubation with **2** was not monitored. Therefore, our studies present that **2** detects Aβ species without influence on the aggregation of Aβ peptides.

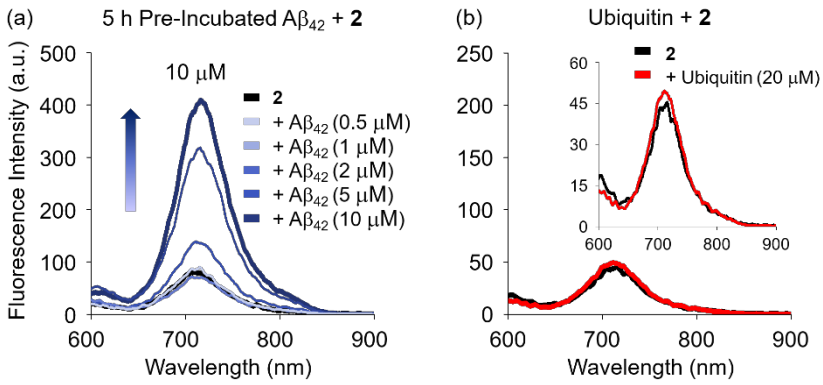

Figure 2.8. Fluorescent responses of **2** towards (a) $A\beta_{42}$ aggregates, generated by pre-incubation for 5 h, and (b) ubiquitin. Conditions: [$A\beta_{42}$] = 0.5, 1, 2, 5, and 10 μM; [ubiquitin] = 20 μM; [**2**] = 2 μM; 20 mM HEPES, pH 7.4, 150 mM NaCl; 10 min incubation with peptides prior to measurements; λ_{ex} = 574 nm.

ULSAN NATIONAL INSTITUTE OF SCIENCE AND TECHNOLOGY

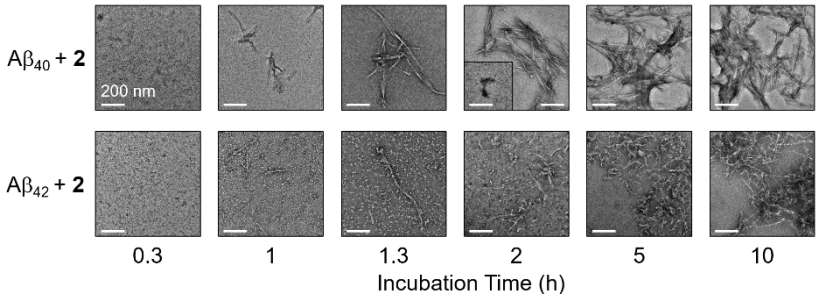

Figure 2.9. Morphologies of Aβ aggregates upon treatment with **2**. The TEM images of pre-incubated (0.3, 1, 1.3, 2, 5, and 10 h) $A\beta_{40}$ (top) and $A\beta_{42}$ (bottom) were obtained after 10 min incubation with **2**. Conditions: [Aβ] = 20 μM; [**2**] = 2 μM; 20 mM HEPES, pH 7.4, 150 mM NaCl. Scale bars = 200 nm.

2.2.5. Imaging of Aβ Aggregates by 2 in Living Cells

To evaluate the ability of **2** to visualize Aβ species in biological environments, imaging of Aβ aggregates by **2** was carried out in 5Y cells (Figure 2.10). No perceptible fluorescence of **2** (λ_{ex} = 594 nm, λ_{em} = 670-770 nm) was shown in the absence of Aβ aggregates in 5Y cells. When the probe was added to the cells pre-treated with $A\beta_{40}$ aggregates generated by pre-incubation for 5 h, a prominent increase in red fluorescence was monitored (Figure 2.10). Note that the extracellularly existing Aβ aggregates and **2** were removed by washing with PBS twice before fixing the cells. The imaging data of **2** with $A\beta_{40}$ aggregates, shown in Figure 2.10, could result from both possibilities: (i) our probe was bound to intracellular Aβ aggregates within the cells; (ii) the assembly of Aβ aggregates with **2** was extracellularly produced and entered the cells. Overall, the imaging results suggest that our probe could present turn-on fluorescence with Aβ aggregates in living cells.

Furthermore, the cytotoxicity of **2** was determined (Figure 2.11). The concentration of **2** (500 nM) used for imaging of Aβ aggregates was nontoxic [98 (±0.6)% of cell viability for 30 min incubation]. Additionally, the IC_{50} value of **2** in 5Y cells for 24 h incubation is 3.3 μM (IC_{50}, the concentration that produces 50% cytotoxicity; Figure 2.11). Thus, our *in vitro* and cell imaging studies propose that **2** could be a turn-on fluorescent probe for monitoring Aβ species in both aqueous media and living cells.

ULSAN NATIONAL INSTITUTE OF SCIENCE AND TECHNOLOGY

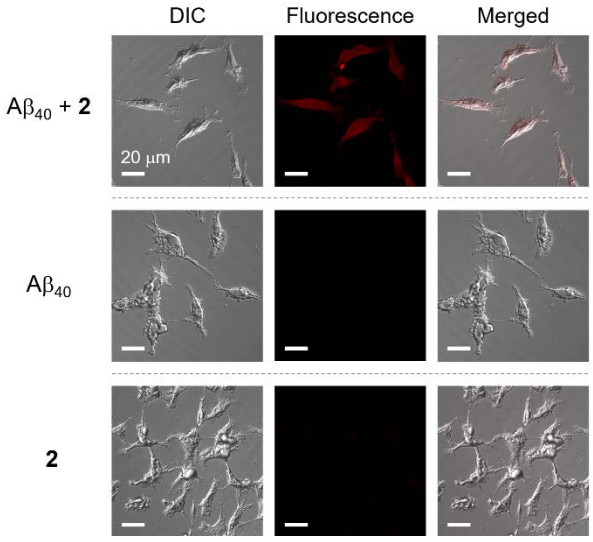

Figure 2.10. Imaging of Aβ aggregates by **2** in living cells. Fluorescent response of **2** was detected upon 30 min incubation with 5Y cells with and without $A\beta_{40}$ aggregates that were generated for 5 h. Conditions: $[A\beta_{40}]$ = 5 μM; [**2**] = 500 nM; λ_{ex} = 594 nm, λ_{em} = 670-770 nm. Scale bars = 20 μm.

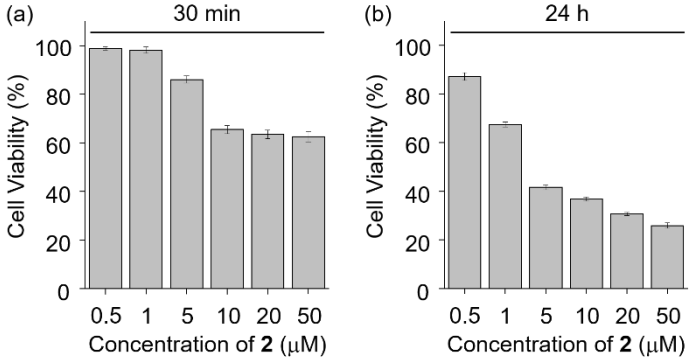

Figure 2.11. Cytotoxicity of **2**. Cell viability (%) of 5Y cells incubated with various concentrations of **2** was calculated through the MTT assay. **2** was treated in 5Y cells and incubated for (a) 30 min and (b) 24 h. The cell viability was determined relative to that of the cells treated with an equivalent amount of DMSO. Error bars indicate the standard error from four independent experiments. Conditions: [**2**] = 0.5, 1, 5, 10, 20, and 50 μM (1% v/v DMSO).

2.3. Conclusion

A fluorescent probe containing the groups of styrene and benzo[*e*]indole was designed and prepared for detecting Aβ species. The fluorescent intensity of the probe, **2**, was increased in the presence of the aggregates of both $A\beta_{40}$ and $A\beta_{42}$ at the near-IR region. According to the aggregation kinetics of Aβ, monitored by the probe, Aβ aggregates were visualized with a noticeable change in turn-on fluorescence. In addition to the aqueous solution, our probe was observed to be useful for visualizing Aβ aggregates

ULSAN NATIONAL INSTITUTE OF SCIENCE AND TECHNOLOGY

in living cells showing turn-on fluorescence. Therefore, our studies present the development and utilization of a near-IR fluorescent probe for indicating Aβ aggregates with turn-on signals. Our probe, however, is positively charged, which limits its blood-brain barrier permeability, similar to ThT[31]. To further advance the utility of such a probe towards Aβ aggregates *in vivo* (particularly, in the brain), we will design structurally modified or new probes with a neutral form, investigate their reactivities, and conduct their histological study, along with confirmation of utilization in biology in the near future.

2.4 Experimental Section

2.4.1. Materials

All chemical reagents were purchased from commercial suppliers and used as received unless otherwise stated. $A\beta_{40}$ (DAEFRHDSGYEVHHQKLVFFAEDVGSNKGAIIGLMVGGVV) and $A\beta_{42}$ (DAEFRHDSGYEVHHQKLVFFAEDVGSNKGAIIGLMVGGVVIA) were purchased from Anaspec (Fremont, CA, USA). Ubiquitin (MQIFVKTLTGKTITLEVEPSDTIENVKAKIQDKEGIPPDQQRLI-FAGKQLEDGRTLSDYNIQKESTLHLVLRLRGG) was obtained from Sigma-Aldrich (St. Louis, MO, USA). HEPES [N-(2-hydroxyethyl)-piperazine-N'-(2-ethanesulfonic acid)] was purchased from Sigma-Aldrich. The buffered solution containing 20 mM HEPES and 150 mM NaCl was prepared in doubly distilled water [ddH_2O; a Milli-Q Direct 16 system (18.2 MΩ cm; Merck KGaA, Darmstadt, Germany)]. Trace metal contamination was removed from the solutions by treating with Chelex (Sigma-Aldrich).

2.4.2. Synthesis of 2 (2-((1E,3E)-4-(4-(dimethylamino)phenyl)buta-1,3-dien-1-yl)-1,1,3-trimethyl-1H-benzo[*e*]indol-3-ium iodide)

To a solution of 4-(dimethylamino)-cinnamaldehyde (1.5 mmol) and 1,1,2,3-tetramethyl-1H-benzo[*e*]indole iodide (1.5 mmol) in ethanol, piperidine (40 μL) was added and the reaction mixture was refluxed for 4 h. After cooled down to room temperature, the solution was treated with diethyl ether. The resulting precipitate was filtered and washed with ethanol and diethyl ether and dried in vacuum (508 mg; yield 80%). ^{1}H NMR (400 MHz; DMSO-d_6; ppm): 1.95 (s, 6H), 3.08 (s, 6H), 4.02 (s, 3H), 6.84 (d, J = 8.9 Hz, 2H), 7.03 (d, J = 15.0 Hz, 1H), 7.31 (t, J = 11.2 Hz, 1H), 7.60 (d, J = 8.9 Hz, 2H), 7.66 (t, J = 8.1 Hz, 1H), 7.72-7.78 (m, 2H), 8.00 (d, J = 8.9 Hz, 1H), 8.17 (d, J = 8.1 Hz, 1H), 8.23 (d, J = 8.9 Hz, 1H), 8.34-8.41 (m, 2H). ^{13}C NMR (125 MHz; DMSO-d_6; ppm): 26.5, 39.8, 40.1, 53.3, 181.0, 160.9, 160.7, 155.6, 153.4, 151.9, 140.3, 137.2, 133.3, 132.0, 131.3, 130.7, 151.9, 127.6, 127.1, 124.6, 123.8, 122.0, 113.5, 112.6, 111.9. MALDI-TOF (m/z): Calcd. for $C_{27}H_{29}N_2$ + 381.23. Found 381.25. Anal.Calcd. for $C_{27}H_{29}N_2I$: C, 63.78%, H, 5.75%, N, 5.51%. Found C, 63.93%, H, 5.70%, N, 5.41%.

2.4.3. Absorption and Emission Measurements

ULSAN NATIONAL INSTITUTE OF SCIENCE AND TECHNOLOGY

The samples of **2** for absorption and emission measurements were prepared in 10 mM phosphate buffered saline (PBS) buffer (pH 7.4), acetonitrile (CH_3CN), and the mixture of methanol (MeOH) and glycerol with different ratios. Absorbance spectra were collected using a PerkinElmer model Lambda 2S UV–Vis spectrophotometer (PerkinElmer, Waltham, MA, USA) and an Agilent 8453 UV–Vis spectrophotometer (Santa Clara, CA, USA). Emission spectra were recorded on a PerkinElmer LS55 fluorescence spectrometer (PerkinElmer) and a HORIBA PTI QuantaMaster 8000 fluorometer (HORIBA, Kyoto, Japan).

2.4.4. Calculation of Quantum Yield

The quantum yield of **2** was calculated using methylene blue as a reference.

$$\mathrm{QY} = \mathrm{QY_{ref}} \frac{\eta^2 \, I \, A_{ref}}{{\eta_{ref}}^2 I_{ref} A}$$

Where QY_{ref} is the quantum yield of the reference compound, η is the refractive index of the solvent, I is the integrated fluorescent intensity, and A is the absorbance at the excitation wavelength. Aβ peptides (0.5 mg/mL) were prepared in 10 mM PBS buffer, pH 7.4 and then incubated at 37 °C for 42 h with constant agitation.

2.4.5. Preparation of Aβ Aggregates and Ubiquitin

The concentrations of Aβ and ubiquitin were determined by an Agilent 8453 UV–Vis spectrophotometer. Aβ peptides were dissolved in hexafluoro-2-propanol (HFIP) and sonicated for 30 min. After evaporation of HFIP for 2 h, Aβ peptides were dissolved in NH_4OH (1% v/v, aq; 10 μL) followed by dilution in ddH_2O. Ubiquitin was dissolved in ddH_2O. The concentration of each peptide was determined by measuring the absorbance of the solution at 280 nm (ε = 1450 $M^{-1}cm^{-1}$ for $Aβ_{40}$; ε = 1490 $M^{-1}cm^{-1}$ for $Aβ_{42}$; ε = 1280 $M^{-1}cm^{-1}$ for ubiquitin). The solution of peptide was diluted to 20 mM with the buffered solution. The Aβ samples were incubated at 37 °C for various time points with constant agitation.

2.4.6. Fluorescence Measurements with Aβ Aggregates

The fluorescent responses of **2** (2 μM; 1% v/v DMSO) to (i) $Aβ_{40}$ and $Aβ_{42}$ species (20 μM), generated at incubation time points (0, 1, 1.3, 1.6, 2, 3, 5, 10, and 12 h); (ii) Aβ42 (0.5, 1, 2, 5, and 10 μM; 5 h incubation); (iii) ubiquitin (20 μM) were measured by a Varian CARY Eclipse fluorescence spectrophotometer [Ulsan National Institute of Science and Technology (UNIST) Central Research

ULSAN NATIONAL INSTITUTE OF SCIENCE AND TECHNOLOGY

Facilities (UCRF), UNIST, Ulsan, Republic of Korea] at λ_{ex} = 574 nm with 10 min incubation prior to measurements.

2.4.7. ThT Assay

The kinetic of forming β-sheet-rich Aβ aggregates was monitored by the ThT assay[34]. ThT (20 μM) was treated with Aβ samples (20 μM) obtained after different incubation time points (0, 0.3, 0.6, 1, 1.3, 1.6, 2, 3, 5, 10, and 12 h) at 37 °C with constant agitation. After 20 min, the fluorescence intensity of ThT (λ_{ex} = 440 nm; λ_{em} = 490 nm) was measured by a SpectraMax M5e microplate reader (Molecular Devices, San Jose, CA, USA).

2.4.8. Dot Blot Assay

The solutions of Aβ aggregates (2 μL) were spotted on a nitrocellulose membrane, and the membrane was blocked with the solution of bovine serum albumin (BSA; 3% w/v; RMBIO, Missoula, MT, USA) in Tris-buffered saline containing 0.01% Tween 20 (TBS-T) at room temperature for 2 h. The membrane was incubated with a primary antibody, 6E10 (1:2000; Covance, Princeton, NJ, USA), A11 (1:1000; Invitrogen, Carlsbad, CA, USA), or OC (1:1000; Merck Millipore, Billerica, MA, USA), in the solution of BSA (2% w/v in TBS-T) for 2 h at room temperature. After washing with TBS-T (3×, 7 min), the horseradish peroxidase-conjugated goat anti-mouse (1:2000; for 6E10; Cayman Chemical Company, Ann Arbor, MI, USA) or goat anti-rabbit (1:2500; for A11 and OC; Promega, Madison, WI, USA) secondary antibody in the solution of BSA (2% w/v in TBS-T) was introduced to the membrane and incubated for 2 h at room temperature. A homemade ECL kit[35-37] was used to visualize the results on a ChemiDoc MP Imaging System (Bio-Rad, Hercules, CA, USA). The same membrane was stripped by treating with hydrogen peroxide (H_2O_2) for 30 min at room temperature, washed with TBS-T (4×, 10 min), blocked with the solution of BSA (3% w/v in TBS-T), and incubated with the other primary antibody (6E10, A11, or OC).

2.4.9. Transmission Electron Microscopy

Aβ samples for TEM measurements were prepared following previously reported methods[35,36,38-40]. Glow discharged grids (Formvar/Carbon 300-mesh, Electron Microscopy Sciences, Hatfield, PA,USA) were treated with the samples (5 μL) of (i) compound-free Aβ aggregates and (ii) Aβ aggregates incubated with **2** for 2 min at room temperature. Excess sample was removed with filter paper and the grids were washed with ddH_2O (3×). Each grid was stained with uranyl acetate (1% w/v ddH_2O; 5 μL) for 1 min. Uranyl acetate was blotted off and grids were dried for 20 min at room temperature. Images of samples were obtained by a JEOL JEM-2100 transmission electron microscope (200 kV; 25,000×

ULSAN NATIONAL INSTITUTE OF SCIENCE AND TECHNOLOGY

magnification; UCRF). The major species of Aβ aggregates are presented among collected images of sample.

2.4.10. Live-Cell Fluorescence Imaging

The human neuroblastoma SH-SY5Y (5Y) cell line [American Type Cell Collection (ATCC), Manassas, VA, USA] was maintained in media containing 1:1 Minimum Essential Media (MEM; GIBCO, Grand Island, NY, USA) and Ham's F12K Kaighn's Modification Media (F12K; GIBCO), 10% (v/v) fetal bovine serum (FBS; Sigma-Aldrich), and 100 U/mL penicillin and 100 mg/mL streptomycin (GIBCO). The 5Y cells were grown in a humidified atmosphere with 5% CO_2 at 37 °C, seeded onto a plate at a density of 70,000 cells per 100 μL, and then incubated at 37 °C for 16 h. The 5Y cells were first treated with **2** [500 nM; final concentration of DMSO (1% v/v)] for 30 min without Aβ aggregates. The cells were washed with PBS (pH 7.4, GIBCO) twice. The cells were fixed with 4% formaldehyde and cold methanol[41] and the fluorescence images were obtained. In the case of $A\beta_{40}$, $A\beta_{40}$ aggregates (5 μM) generated by pre-incubation for 5 h were treated to the cells for 1 h prior to the addition of **2** (500 nM). After 30 min incubation of **2**, the cells were washed with PBS twice. After fixation, images were obtained by a confocal microscope Carl Zeiss LSM780 [Korea Advanced Institute of Science and Technology (KAIST) Analysis center for Research Advancement (KARA), KAIST, Daejeon, Republic of Korea]. The images were obtained by 561 nm laser with Alexa Fluor 594 detection channel with modification of emission collecting range from 670 to 770 nm (2.0% power; 1.58 μs as the pixel dwell; 57 nm as the pinhole size; 63× objective).

2.4.11. Cell Viability Studies

Cell viability upon treatment with **2** was determined by the MTT assay. 5Y cells were seeded in a 96-well plate (10,000 cells in 100 μL per well). The cells were treated with compounds (0.5, 1, 5, 10, 20, and 50 μM; 1% v/v final DMSO concentration) and incubated for 30 min and 24 h. After incubation, MTT [25 μL; 5 mg/mL in PBS (pH 7.4)] was added to each well and the plate was incubated for 4 h at 37 °C. Formazan produced by the cells was solubilized using an acidic solution of *N*,*N*-dimethylformamide (DMF; 50% v/v, aq) and sodium dodecyl sulfate (SDS; 20% w/v) overnight at room temperature in the dark. The absorbance was measured at 600 nm by a microplate reader.

2.5. Acknowledgments

This work is supported by “Next Generation Carbon Upcycling Project” [Project No. 2017M1A2A2042517 (to J.K.)] through the National Research Foundation (NRF) funded by the Ministry of Science and ICT and the NRF grant funded by the Korean government [NRF-

ULSAN NATIONAL INSTITUTE OF SCIENCE AND TECHNOLOGY

2017R1A5A1015365 (to J.K.); NRF-2016R1A5A1009405 and NRF-2017R1A2B3002585 (to M.H.L.)].

2.6. References

1. Murphy, M. P.; LeVine, H., III, *J. Alzheimers Dis.* **2010**, *19*, 311-323.
2. Hamley, I. W., *Chem. Rev.* **2012**, *112*, 5147-5192.
3. Kepp, K. P., *Chem. Rev.* **2012**, *112*, 5193-5239.
4. Bernstein, S. L.; Dupuis, N. F.; Lazo, N. D.; Wyttenbach, T.; Condron, M. M.; Bitan, G.; Teplow, D. B.; Shea, J. E.; Ruotolo, B. T.; Robinson, C. V.; Bowers, M. T., *Nat. Chem.* **2009**, *1*, 326-331.
5. Ahmed, M.; Davis, J.; Aucoin, D.; Sato, T.; Ahuja, S.; Aimoto, S.; Elliott, J. I.; Van Nostrand, W. E.; Smith, S. O., *Nat. Struct. Mol. Biol.* **2010**, *17*, 561-567.
6. Rajasekhar, K.; Chakrabarti, M.; Govindaraju, T., *Chem. Commun.* **2015**, *51*, 13434-13450.
7. Lee, S. J. C.; Nam, E.; Lee, H. J.; Savelieff, M. G.; Lim, M. H., *Chem. Soc. Rev.* **2017**, *46*, 310-323.
8. Sakono, M.; Zako, T., *FEBS J.* **2010**, *277*, 1348-1358.
9. Savelieff, M. G.; Lee, S.; Liu, Y.; Lim, M. H., *ACS Chem. Biol.* **2013**, *8*, 856-865.
10. Tsai, J.; Grutzendler, J.; Duff, K.; Gan, W. B., *Nat. Neurosci.* **2004**, *7*, 1181-1183.
11. Biancalana, M.; Koide, S., *Biochim. Biophys. Acta* **2010**, *1804*, 1405-1412.
12. Rajasekhar, K.; Narayanaswamy, N.; Murugan, N. A.; Viccaro, K.; Lee, H. G.; Shah, K.; Govindaraju, T., *Biosens. Bioelectron.* **2017**, *98*, 54-61.
13. Rajasekhar, K.; Narayanaswamy, N.; Murugan, N. A.; Kuang, G.; Agren, H.; Govindaraju, T., *Sci. Rep.* **2016**, *6*, 23668.
14. Zhang, X.; Tian, Y.; Zhang, C.; Tian, X.; Ross, A. W.; Moir, R. D.; Sun, H.; Tanzi, R. E.; Moore, A.; Ran, C., *Proc. Natl. Acad. Sci. U. S. A.* **2015**, *112*, 9734-9739.
15. Zhu, B. Y.; Cheng, Y.; Li, G. B.; Yang, S. Y.; Zhang, Z. R., *Bioorg. Med. Chem.* **2016**, *24*, 827-834.
16. Hintersteiner, M.; Enz, A.; Frey, P.; Jaton, A. L.; Kinzy, W.; Kneuer, R.; Neumann, U.; Rudin, M.; Staufenbiel, M.; Stoeckli, M.; Wiederhold, K. H.; Gremlich, H. U., *Nat. Biotechnol.* **2005**, *23*, 577-583.
17. Cui, M.; Ono, M.; Watanabe, H.; Kimura, H.; Liu, B.; Saji, H., *J. Am. Chem. Soc.* **2014**, *136*, 3388-3394.
18. Ran, C.; Xu, X.; Raymond, S. B.; Ferrara, B. J.; Neal, K.; Bacskai, B. J.; Medarova, Z.; Moore, A., *J. Am. Chem. Soc.* **2009**, *131*, 15257-15261.
19. Cheng, Y.; Zhu, B.; Deng, Y.; Zhang, Z., *Anal. Chem.* **2015**, *87*, 4781-4787.
20. Zhang, X.; Tian, Y.; Li, Z.; Tian, X.; Sun, H.; Liu, H.; Moore, A.; Ran, C., *J. Am. Chem. Soc.* **2013**, *135*, 16397-16409.

ULSAN NATIONAL INSTITUTE OF SCIENCE AND TECHNOLOGY

21. Raymond, S. B.; Skoch, J.; Hills, I. D.; Nesterov, E. E.; Swager, T. M.; Bacskai, B. J., *Eur. J. Nucl. Med. Mol. Imaging* **2008**, *35*, S93-98.
22. Okamura, N.; Mori, M.; Furumoto, S.; Yoshikawa, T.; Harada, R.; Ito, S.; Fujikawa, Y.; Arai, H.; Yanai, K.; Kudo, Y., *J. Alzheimers Dis.* **2011**, *23*, 37-48.
23. Fu, H.; Cui, M.; Tu, P.; Pan, Z.; Liu, B., *Chem. Commun.* **2014**, *50*, 11875-11878.
24. Kim, D.; Moon, H.; Baik, S. H.; Singha, S.; Jun, Y. W.; Wang, T.; Kim, K. H.; Park, B. S.; Jung, J.; Mook-Jung, I.; Ahn, K. H., *J. Am. Chem. Soc.* **2015**, *137*, 6781-6789.
25. Sozmen, F.; Kolemen, S.; Kumada, H. O.; Ono, M.; Saji, H.; Akkaya, E. U., *RSC Adv.* **2014**, *4*, 51032-51037.
26. Tong, H.; Lou, K.; Wang, W., *Acta Pharm. Sin. B* **2015**, *5*, 25-33.
27. Zhu, J. Y.; Zhou, L. F.; Li, Y. K.; Chen, S. B.; Yan, J. W.; Zhang, L., *Anal. Chim. Acta* **2017**, *961*, 112-118.
28. Rajasekhar, K.; Govindaraju, T., *RSC Adv.* **2018**, *8*, 23780-23804.
29. Staderini, M.; Martin, M. A.; Bolognesi, M. L.; Menendez, J. C., *Chem. Soc. Rev.* **2015**, *44*, 1807-1819.
30. Liu, H.; Yang, J.; Wang, L.; Xu, Y.; Zhang, S.; Lv, J.; Ran, C.; Li, Y., *Future Med. Chem.* **2017**, *9*, 179-198.
31. Nesterov, E. E.; Skoch, J.; Hyman, B. T.; Klunk, W. E.; Bacskai, B. J.; Swager, T. M., *Angew. Chem. Int. Ed. Engl.* **2005**, *44*, 5452-5456.
32. Kim, S.; Lee, H. J.; Nam, E.; Jeong, D.; Cho, J.; Lim, M. H.; You, Y., *ACS Omega* **2018**, *3*, 5141-5154.
33. Samanta, S.; Dey, P.; Ramesh, A.; Das, G., *Chem. Commun.* **2016,** *52*, 10381-10384.
34. LeVine, H., III, *Protein Sci.* **1993**, *2*, 404-410.
35. Beck, M. W.; Derrick, J. S.; Kerr, R. A.; Oh, S. B.; Cho, W. J.; Lee, S. J.; Ji, Y.; Han, J.; Tehrani, Z. A.; Suh, N.; Kim, S.; Larsen, S. D.; Kim, K. S.; Lee, J. Y.; Ruotolo, B. T.; Lim, M. H., *Nat. Commun.* **2016**, *7*, 13115.
36. Lee, H. J.; Korshavn, K. J.; Nam, Y.; Kang, J.; Paul, T. J.; Kerr, R. A.; Youn, I. S.; Ozbil, M.; Kim, K. S.; Ruotolo, B. T.; Prabhakar, R.; Ramamoorthy, A.; Lim, M. H., *Chem. Eur. J.* **2017**, *23*, 2706-2715.
37. Mruk, D. D.; Cheng, C. Y., *Spermatogenesis* **2011**, *1*, 121-122.
38. Derrick, J. S.; Kerr, R. A.; Nam, Y.; Oh, S. B.; Lee, H. J.; Earnest, K. G.; Suh, N.; Peck, K. L.; Ozbil, M.; Korshavn, K. J.; Ramamoorthy, A.; Prabhakar, R.; Merino, E. J.; Shearer, J.; Lee, J. Y.; Ruotolo, B. T.; Lim, M. H., *J. Am. Chem. Soc.* **2015**, *137*, 14785-14797.
39. Derrick, J. S.; Kerr, R. A.; Korshavn, K. J.; McLane, M. J.; Kang, J.; Nam, E.; Ramamoorthy, A.; Ruotolo, B. T.; Lim, M. H., *Inorg. Chem.* **2016**, *55*, 5000-5013.
40. Derrick, J. S.; Lee, J.; Lee, S. J.; Kim, Y.; Nam, E.; Tak, H.; Kang, J.; Lee, M.; Kim, S. H.; Park,

ULSAN NATIONAL INSTITUTE OF SCIENCE AND TECHNOLOGY

K.; Cho, J.; Lim, M. H., *J. Am. Chem. Soc.* **2017**, *139*, 2234-2244.

41. Nam, J. S.; Kang, M. G.; Kang, J.; Park, S. Y.; Lee, S. J.; Kim, H. T.; Seo, J. K.; Kwon, O. H.; Lim, M. H.; Rhee, H. W.; Kwon, T. H., *J. Am. Chem. Soc.* **2016**, *138*, 10968-10977.
42. Sutharsan, J.; Dakanali, M.; Capule, C. C.; Haidekker, M. A.; Yang, J.; Theodorakis, E. A., *ChemMedChem* **2010**, *5*, 56-60.
43. Derrick, J. S.; Lim, M. H., *ChemBioChem* **2015**, *16*, 887-898.
44. DeToma, A. S.; Salamekh, S.; Ramamoorthy, A.; Lim, M. H., *Chem. Soc. Rev.* **2012**, *41*, 608-621.
45. Teoh, C. L.; Su, D.; Sahu, S.; Yun, S. W.; Drummond, E.; Prelli, F.; Lim, S.; Cho, S.; Ham, S.; Wisniewski, T.; Chang, Y. T., *J. Am. Chem. Soc.* **2015**, *137*, 13503-13509.
46. Lv, G.; Sun, A.; Wei, P.; Zhang, N.; Lan, H.; Yi, T., *Chem. Commun.* **2016**, *52*, 8865-8868.
47. Lee, Y. O.; Shin, J. W.; Yi, C.; Lee, Y. H.; Sohn, N. W.; Kang, C.; Kim, J. S., *Chem. Commun.* **2014**, *50*, 5741-5744.
48. Yang, H. Y.; Zhang, J. J.; Zang, Y.; Zhang, H. Y.; Li, J.; Chen, G. R.; He, X. P., *Dyes Pigm.* **2017**, *136*, 224-228.
49. Liu, K.; Guo, T. L.; Chojnacki, J.; Lee, H. G.; Wang, X.; Siedlak, S. L.; Rao, W.; Zhu, X.; Zhang, S., *ACS Chem. Neurosci.* **2012**, *3*, 141-146.
50. Stsiapura, V. I.; Maskevich, A. A.; Kuzmitsky, V. A.; Uversky, V. N.; Kuznetsova, I. M.; Turoverov, K. K., *J. Phys. Chem. B* **2008**, *112*, 15893-15902.
51. Levitt, J. A.; Chung, P. H.; Kuimova, M. K.; Yahioglu, G.; Wang, Y.; Qu, J.; Suhling, K., *ChemPhysChem* **2011**, *12*, 662-672.
52. Peccati, F.; Hernando, J.; Blancafort, L.; Solans-Monfort, X.; Sodupe, M., *Phys. Chem. Chem. Phys.* **2015**, *17*, 19718-19725.
53. Amdursky, N.; Huppert, D., *J. Phys. Chem. B.* **2012**, *116*, 13389-13395.
54. Kayed, R.; Head, E.; Sarsoza, F.; Saing, T.; Cotman, C. W.; Necula, M.; Margol, L.; Wu, J.; Breydo, L.; Thompson, J. L.; Rasool, S.; Gurlo, T.; Butler, P.; Glabe, C. G., *Mol. Neurodegener* **2007**, *2*, 18.
55. Kayed, R.; Head, E.; Thompson, J. L.; McIntire, T. M.; Milton, S. C.; Cotman, C. W.; Glabe, C. G., *Science* **2003**, *300*, 486-489.
56. Pickart, C. M.; Eddins, M. J., *Biochim. Biophys. Acta* **2004**, *1695*, 55-72.

ULSAN NATIONAL INSTITUTE OF SCIENCE AND TECHNOLOGY

Chapter 3.

Detection of Metal Ions by Fluorescent Probes in Living Cells

The results illustrated in this Chapter were recently published: (1) Suh Mi Hwang, Min Seon Kim, Misun Lee, Mi Hee Lim, and Cheal Kim, *New J. Chem.* **2017**, *41*, 15590-15600; (2) Hyo Jung Jang, Ji Hye Kang, Misun Lee, Mi Hee Lim, and Cheal Kim, *Ind. Eng. Chem. Res.* **2018**, *57*, 54-62; (3) Hyo Jung Jang, Ahran, Kim, Jae Min Jung, Misun Lee, Mi Hee Lim, and Cheal Kim, *Bull. Korean Chem. Soc.* **2018**, In Press (DOI: 10.1002/bkcs.11608). I performed live-cell imaging experiments.

ULSAN NATIONAL INSTITUTE OF SCIENCE AND TECHNOLOGY

3.1. Introduction

Metal ions are essential components in our body for catalytic and structural functions in metalloenzymes, cellular signaling transmission, and metabolic process[1,2]. The distribution and concentration of metal ions are tightly regulated throughout cellular systems to maintain their homeostasis of biological systems[1,3]. Indeed, numerous studies have suggested that dysregulation of metal ions is significantly implicated in the pathogenesis of neurodegenerative diseases[2,4,5]. Highly concentrated metal ions can trigger the generation of reactive oxygen species which induce oxidative damage to cellular components, eventually leading to neuronal death[2,4]. Moreover, the elevated level of metal ions in the brain can attribute to accelerate the aggregation of proteins or inhibiting their enzymatic activities, inducing neurotoxicity[4,6]. To elucidate the complex metal-associated physiopathology in neurodegenerative diseases, effective techniques to provide information about metal-related biological events is necessary. Fluorescence-based detection of metal ions by chemical probes is a practical method to non-invasively indicate their local concentration and quantity in biological sytems[7,8]. In this Chapter, we evaluated the ability of the newly developed chemical probes capable of selectively responding to Al^{3+} and Zn^{2+} ions, respectively, with distinct fluorescence in living cells.

3.2. Results and Discussion

3.2.1. Detection of Al^{3+} Using the Probe, 3, in Living Cells

A fluorescent sensor for Al^{3+}, **3**, was designed through the linkage of diethylaminophenol, as an electron donating group with high water solubility, and 2-furoic hydrazide, as a metal chelating moiety (Scheme 3.1). The selective fluorescent response of **3** to Al^{3+} was monitored in an aqueous system at *ca.* 450 nm, and their photophysical property (*e.g.*, stoichiometry and detection limits) and potential binding modes were determined. To assess the applicability of **3** as a sensor for Al^{3+} in biological environments, the fluorescent response of **3** was observed in HeLa cells in the absence and presence of Al^{3+}. Prior to the introduction of **3**, Al^{3+} (500 μM) was treated to HeLa cells followed by 20 min incubation. Without **3**, any significant fluorescence was not exhibited in living cells. In contrast, a noticeable increase in fluorescence was observed upon treatment of **3** (25 μM) at the region of 4′,6-diamidino-2-phenylindole (DAPI) channel [λ_{ex} = 357 (± 22) nm; λ_{em} = 447 (± 30) nm] (Figure. 3.1). These results demonstrate **3** as a turn-on chemosensor for detecting Al^{3+} in biological systems.

ULSAN NATIONAL INSTITUTE OF SCIENCE AND TECHNOLOGY

Scheme 3.1. Proposed binding mode of **3** with Al^{3+}.

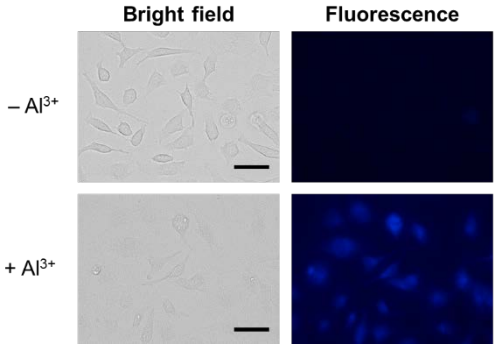

Figure 3.1. Fluorescence imaging of HeLa cells incubated with **3** and Al^{3+}. Cells were pre-incubated with Al^{3+} for 20 min prior to the addition of **3**. Conditions: [**3**] = 25 μM, [Al^{3+}] = 500 μM, 37 °C, 5% CO_2. Scale bars = 50 μm.

3.2.2. Detection of Zn^{2+} Using the Probe, 4, in Living Cells

A new turn-on fluorescent probe for Zn^{2+}, **4**, was designed and synthesized. **4** showed the noticeable enhancement in fluorescence upon treatment of Zn^{2+} at *ca.* 520 nm, and its detection limits and the possible binding mode were identified in aqueous media (Scheme 3.2). To determine **4**'s bioapplicability as a sensor for Zn^{2+} in living cells, the fluorescent response and cytotoxicity were measured in HeLa cells. When **4** (10 μM) was pre-incubated with living cells for 5 min followed by treatment with Zn^{2+} (1 mM), noticeable turn-on fluorescence was indicated at the range of green fluorescent protein (GFP) channel [λ_{ex} = 470 (± 11) nm; λ_{em} = 510 (± 21) nm] (Figure 3.2). Under our imaging conditions ([**4**] = 10 μM; 5 min incubation), no toxicity of **4** was observed. These results suggest the potential use of **4** for detection of Zn^{2+} in cellular environments.

ULSAN NATIONAL INSTITUTE OF SCIENCE AND TECHNOLOGY

Scheme 3.2. Possible binding mode of the **4**–Zn^{2+} complex.

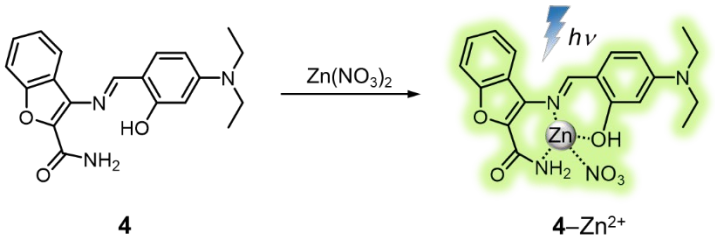

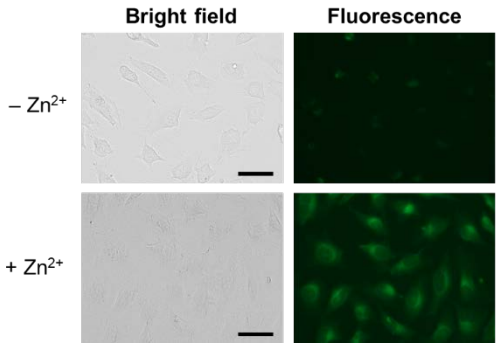

Figure 3.2. Fluorescence imaging of HeLa cells incubated with **4** and Zn^{2+}. Cells were incubated with **4** and Zn^{2+} for 5 min. Conditions: [**4**] = 10 μM; [Zn^{2+}] = 1 mM; 37 °C; 5% CO_2. Scale bars = 50 μm.

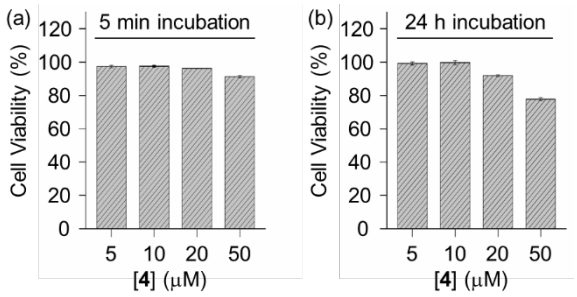

Figure 3.3. Toxicity of **4** incubated in HeLa cells for (a) 5 min and (b) 24 h. **4** was treated to HeLa cells at various concentrations (5, 10, 20, and 50 μM; 1% v/v DMSO). Cell viability (%) was determined by the MTT assay [MTT = 3-(4,5-dimethylthiazol-2-yl)-2,5-diphenyltetrazolium bromide] in comparison to that of cells treated with DMSO only (1% v/v). Error bars represent the standard error from three independent experiments.

3.2.3. Detection of Zn^{2+} Using the Probe, 5, in Living Cells

A selective Zn^{2+} chemosensor based on benzofuran, **5**, was newly designed and obtained. In aqueous media, **5** exhibited the distinct fluorescent response at *ca.* 530 nm to Zn^{2+} over other metal ions. The potential binding mode of **5**–Zn^{2+} was determined through multiple spectroscopic and spectrometric studies (*e.g.*, NMR, ESI-MS, and UV–Vis). In HeLa cells, **5** was pre-treated for 90 min prior to addition of Zn^{2+}. In the presence of both **5** and Zn^{2+}, a significant increase in fluorescence was observed in HeLa

ULSAN NATIONAL INSTITUTE OF SCIENCE AND TECHNOLOGY

cells. As the concentration of Zn^{2+} increased (0 to 1 mM), the clearer shape of cells was observed showing enhanced fluorescence. Our observation reveals **5**'s capability of monitoring Zn^{2+} in living cells.

Scheme 3.3. Proposed binding mode of **5** with Zn^{2+}.

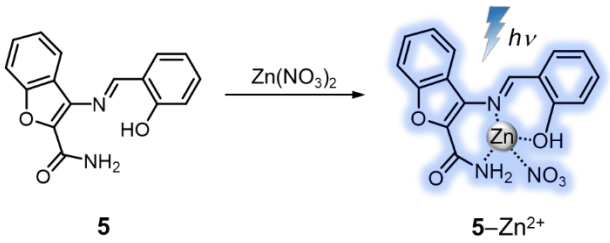

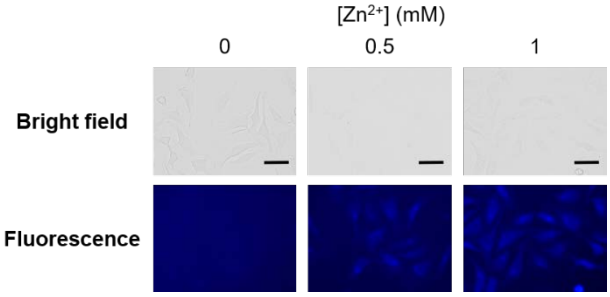

Figure 3.4. Fluorescence images of HeLa cells incubated with **5** followed by the addition of Zn^{2+}. Cells were treated with **5** for 90 min prior to the introduction of Zn^{2+}. Conditions: [**5**] = 25 μM; [Zn^{2+}] = 0.5 or 1 mM; 37 °C; 5% CO_2. Scale bars = 50 μm.

3.3. Conclusion

Metal ions play important biological roles in various functions in our body; thus, their dyshomeostasis is significantly contributed to the initiation and progression of neurodegeneration[2,4,5]. To effectively uncover the metal-associated pathogenesis of neurodegenerative diseases, many researchers have focused on the development of fluorescent probes to monitor metal ions in biological systems. In our studies, we newly developed and utilize the probes (*i.e.*, **3**, **4**, and **5**) for detecting each metal ion (*i.e.*, Al^{3+} and Zn^{2+}) in living cells. Further structural modifications will be carried out to improve high specificity, selectivity, and safety for biological applications.

ULSAN NATIONAL INSTITUTE OF SCIENCE AND TECHNOLOGY

3.4. Experimental Section

3.4.1. Imaging Experiments in Living Cells

HeLa cells (ATCC, Manassas, VA, USA) were maintained in media containing Dulbecco's Modified Eagle's Medium (DMEM), 10% fetal bovine serum (FBS; Sigma-Aldrich), 100 U/mL penicillin and 100 mg/mL streptomycin (GIBCO, Grand Island, NY, USA). The cells were grown in a humidified atmosphere containing 5% CO_2 at 37 °C. Cells were seeded onto a 12-well plate (SPL Life Sciences Co., Ltd, Republic of Korea) and then incubated at 37 °C. Cells were treated with various concentration of $Al(NO_3)_3$ or $Zn(NO_3)_2$ (dissolved in water; 1% v/v final concentration) and probes (**3**, **4**, or **5**; in DMSO; 1% v/v final concentration). Imaging was obtained using an EVOS FL fluorescence microscope (Life Technologies) using a light cube of DAPI [λ_{ex} = 357 (± 22) nm; λ_{em} = 447 (± 30) nm] or GFP [λ_{ex} = 470 (± 11) nm; λ_{em} = 510 (± 21) nm].

3.4.2. Cell Viability Study of **4**.

HeLa cells were grown and maintained at 37 °C in a humidified atmosphere with 5% CO_2. Cell viability upon treatment with **4** was determined by the MTT assay. Cells were seeded in a 96 well plate [(a) 8,000 cells for 5 min incubation and (b) 1,500 cells for 24 h incubation in 100 mL per well]. Cells were treated with various concentrations **4** (5, 10, 20, and 50 μM). After 5 min or 24 h incubation, MTT [25 mL of 5 mg/mL in PBS (pH 7.4, GIBCO)] was added to each well, and the plate was incubated for 4 h at 37 °C. Formazan produced by cells was solubilized using an acidic solution of dimethylformamide (DMF; pH 4.5, 50% v/v, aq) and sodium dodecyl sulfate (SDS; 20% w/v) overnight at room temperature in the dark. The absorbance was measured at 600 nm by the microplate reader. Cell viability was calculated relative to cells containing an equivalent amount of DMSO.

3.5. Acknowledgments

Financial support from National Research Foundation of Korea (NRF) funded by the Ministry of Education, Science and Technology (NRF-2017R1A2B3002585 to M.H.L.).

3.6. References

1. Bleackley, M. R.; Macgillivray, R. T., *Biometals* **2011**, *24*, 785-809.
2. Crichton, R. R.; Dexter, D. T.; Ward, R. J., *Coord. Chem. Rev.* **2008**, *252*, 1189-1199.
3. Roesijadi, G., *Comp. Biochem. Physiol. C Pharmacol. Toxicol. Endocrinol.* **1996**, *113*, 117-123.
4. Bolognin, S.; Messori, L.; Zatta, P., *Neuromolecular Med.* **2009**, *11*, 223-238.
5. Greenough, M. A.; Camakaris, J.; Bush, A. I., *Neurochem. Int.* **2013**, *62*, 540-555.
6. Savelieff, M. G.; Lee, S.; Liu, Y.; Lim, M. H., *ACS Chem. Biol.* **2013**, *8*, 856-865.
7. Ueno, T.; Nagano, T., *Nat. Methods* **2011**, *8*, 642-645.
8. Chan, J.; Dodani, S. C.; Chang, C. J., *Nat. Chem.* **2012**, *4*, 973-984.

ULSAN NATIONAL INSTITUTE OF
SCIENCE AND TECHNOLOGY

Acknowledgments

Finally, with the help of many people who have supported and encouraged me, I was able to complete my master degree.

Above all, I would like to express my gratitude to Professor Lim, my supervisor. With her sincere guidance, dedication, and care about research projects, I was able to focus on my research and gain better academic attitudes. Moreover, I also thank her for giving me opportunities to experience in both outstanding research institutes, UNIST and KAIST, as well as to participate me in various conferences, which extended my view to understand the research and encouraged me intrinsically and extrinsically a lot. I believe all of my experience in Lim group will provide me a good scientific foundation to grow up as an independent researcher and an individual person to dedicate to the society through the scientific knowledge and skills that I learned here.

I appreciate Professor Oh-Hoon Kwon to his kindness to be an advisor. Without his consideration for me, I could not complete my studies for M.S. courses. I thank him a lot for considering and evaluating my works conducted for two years of research. I also would like to appreciate my committee member, Jung-Min Kee for sparing his precious time to assess my thesis and for providing me a helpful advice.

I would like to offer my special thanks to Professor Jae-Sung Bae, Professor Hee Kyung Jin, Professor Joo-Yong Lee, Professor Jinheung Kim, and Professor Cheal Kim giving me opportunities to collaborate with them. Without their assistance, all the studies described in my thesis could not be possible to complete.

I am extremely thankful for my group members who have supported and assisted my research works [Dr. Hyuck Jin Lee, Juhye Kang, Eunju Nam, Geewoo Nam, Jiyeon Han, Mingeun Kim, Nahye Park, Jong-Min Suh, Yelim Yi, Gunhee Kim, and Juri Lee]. It has been grateful for me to study and build up friendships in the Lim group. To the previous members, Jefferey S. Derrick and Yonghwan Ji, I appreciate their help and teaching during the early period of my undergraduate research in the Lim group. In addition, I really thank our lab manager, Ms. Mi Sook Lim, for her tender care in academic administration.

Lastly, I would like to express gratitude to my parents, brother for their great supports and faith to me. With your mental and emotional support, I could keep my way steadily to study for my future.

ULSAN NATIONAL INSTITUTE OF SCIENCE AND TECHNOLOGY

Misun Lee

Department of Chemistry
Ulsan National Institute of Science and Technology (UNIST)
UNIST-gil 50, Ulsan 689-798, Republic of Korea.
Email: lmsun0211@unist.ac.kr

Education

Mar. 2017 – Feb. 2019 **M.S., Chemistry**
Ulsan National Institute of Science and Technology (UNIST)
Ulsan, Republic of Korea
Advisors: Professor Mi Hee Lim & Oh-Hoon Kwon

Mar. 2013 – Feb. 2017 **B.S., Chemistry**
Ulsan National Institute of Science and Technology (UNIST)
Ulsan, Republic of Korea

Honors, Awards, and Scholarships

Mar. 2017 – Aug. 2017 **Teaching Assistant (TA) Scholarships**
Ulsan National Institute of Science and Technology (UNIST),
Ulsan, Republic of Korea

Mar. 2015 – Feb. 2017 **National Scholarship for Excellence**
National Scholarship for Science and Engineering
Korea Student Aid Foundation, Seoul, Republic of Korea

Mar. 2013 – Feb. 2015 **Ulsan National Institute of Science and Technology**
Full-scholarship

Publications

8. Mingeun Kim,[‡] Juhye Kang,[‡] **Misun Lee**,[‡] Jiyeon Han, Geewoo Nam, Eunyoung Tak, Min Sun Kim, Doin Kim, Hyuck Jin Lee, Eunju Nam, Joo-Yong Lee,* and Mi Hee Lim* ([‡]co-first authorship)
Manuscript in Preparation.
"Minimalistic Design Approach for Multi-Reactivity against Free Radicals and Metal-Free and Metal-Bound Amyloid-β Peptides: Redox-Based Substitutions of Benzene"

7. **Misun Lee**,[§] Min Hee Park,[§] Ju Youn Lee, Min Seock Jeong, Kang Ho Park, Seung Hoon Han, Mingeun Kim, Juhye Kang, Geewoo Nam, Eunyoung Tak, Min Sun Kim, Joo-Yong Lee, Hee Kyung Jin,* Jae-Sung Bae,* and Mi Hee Lim* ([§]co-first authorship)
Submitted for Publication, **2019**.
"A neuroprotective small molecule promotes microglial phagocytic aptitude and improves cognitive function"

6. **Misun Lee**,[‡] Mingeun Kim,[‡] Anjong Florence Tikum,[‡] Hyuck Jin Lee, Vijayan Thamilarasan, Mi Hee Lim,* and Jinheung Kim* ([‡]co-first authorship).

ULSAN NATIONAL INSTITUTE OF SCIENCE AND TECHNOLOGY

Dyes Pigm. **2019**, *162*, 97-103.
"A Near-Infrared Fluorescent Probe for Amyloid-β Aggregates"

5. Hyo Jung Jang, Ahran, Kim, Jae Min Jung, **Misun Lee**, Mi Hee Lim, and Cheal Kim*
Bull. Korean Chem. Soc. **2018**, In Press (DOI: 10.1002/bkcs.11608).
"Detection of Zinc(II) by a Fluorescence Chemosensor Based on Benzofuran in Aqueous Media and Live Cells"

4. Masha Savelieff, Geewoo Nam, Juhye Kang, Hyuck Jin Lee, **Misun Lee**, and Mi Hee Lim*
Chem. Rev. **2018**, In Press (DOI: 10.1021/acs.chemrev.8b00138).
"Development of Multifunctional Molecules as Potential Therapeutic Candidates for Alzheimer's Disease, Parkinson's Disease, and Amyotrophic Lateral Sclerosis in the Last Decade"

3. Hyo Jung Jang, Ji Hye Kang, **Misun Lee**, Mi Hee Lim,* and Cheal Kim*
Ind. Eng. Chem. Res. **2018**, *57*, 54-62.
"Fluorescent Sensor for Sequentially Monitoring Zinc(II) and Cyanide Anion in Near-Perfect Aqueous Media"

2. Suh Mi Hwang, Min Seon Kim, **Misun Lee**, Mi Hee Lim, and Cheal Kim*
New J. Chem. **2017**, *41*, 15590-15600.
"Single Fluorescent Chemosensor for Multiple Targets: Sequential Detection of Al^{3+} and Pyrophosphate and Selective Detection of F^- in Near-Perfect Aqueous Solution"

1. Jeffrey S. Derrick, Jiwan Lee, Shin Jung C. Lee, Yujeong Kim, Eunju Nam, Hyeonwoo Tak, Juhye Kang, **Misun Lee**, Sun Hee Kim,* Kiyoung Park,* Jaeheung Cho,* and Mi Hee Lim*
J. Am. Chem. Soc. **2017**, *139*, 2234-2244.
"Mechanistic Insights into Tunable Metal-Mediated Hydrolysis of Amyloid-β Peptides"

Selected Presentations

4. **Poster**, 9th Asian Biological Inorganic Chemistry Conference, UTown, Singapore, December 9-14, 2018
Misun Lee, Mingeun Kim, Anjong Florence Tikum, Hyuck Jin Lee, Vijayan Thamilarasan, Mi Hee Lim*, Jinheung Kim*
"A Near-Infrared Fluorescent Probe for Amyloid-β Aggregates"

3. **Poster**, The 122nd General Meeting of the Korean Chemical Society, Daegu, Korea, October 17-19, 2018
Misun Lee, Mingeun Kim, Anjong Florence Tikum, Hyuck Jin Lee, Vijayan Thamilarasan, Mi Hee Lim*, Jinheung Kim*
"A Near-Infrared Fluorescent Probe for Amyloid-β Aggregates"

2. **Poster**, The Bioinorganic Chemistry Symposium, Daejeon, Korea, August 22-23, 2018
Misun Lee, Mingeun Kim, Anjong Florence Tikum, Hyuck Jin Lee, Vijayan Thamilarasan, Mi Hee Lim*, Jinheung Kim*
"A Near-Infrared Fluorescent Probe for Amyloid-β Aggregates"

ULSAN NATIONAL INSTITUTE OF SCIENCE AND TECHNOLOGY

1. **Poster**, The 2018 Bioinorganic Chemistry Symposium, Suanbo, Korea, July 19-20, 2018
Misun Lee, Mingeun Kim, Anjong Florence Tikum, Hyuck Jin Lee, Vijayan Thamilarasan, Mi Hee Lim*, Jinheung Kim*
"A Near-Infrared Fluorescent Probe for Amyloid-β Aggregates"